Doctoral Dissertation

# Sediment-Loading Processes in a Forested Catchment Influenced by Slope Failure

（斜面崩壊を伴う森林流域の土砂流出機構）

**Md. Motaleb Hossain**

Department of Natural History Sciences
Graduate School of Science
Hokkaido University

November 2015

# Sediment-Loading Processes in a Forested Catchment Influenced by Slope Failure

Md. Motaleb Hossain

Doctoral Thesis

Department of Natural History Sciences
Graduate School of Science
Hokkaido University

November 2015

# ABSTRACT

The “slope failure” in my study means the surface failure and deep landslide on catchment slope and the bank collapse in riparian regions, which occur under rainfall, snowmelt or earthquake. Dynamic processes of landslide on catchment slope have been investigated by many geologists, geomorphologists and geophysicists, but studies on subsequent fluvial sedimentation processes, connected to sediment load of river, are very few in the world. My study area, the Oikamanai River catchment, eastern Hokkaido, is forested (ca. 90% area), but accompanied by two tephra layer (Tarumae Ta-b in 1667 and Shikotsu Spfa-1, 40,000 years ago) in forest soils and the Neogene sedimentary rocks with active faults, which tend to frequently produce surface failure and deep landslide, respectively, under heavy rainfall or snowmelt. In order to understand and predict such disastrous phenomena and subsequent fluvial sedimentation in the catchment, I monitored water level and water turbidity of river in the Oikamanai River catchment in rainfall seasons of 2011 – 2014, and modeled observed discharge and sediment load time series. The turbidity and river-stage monitoring were performed at two sites along the river, and thereby, I distinguished rainfall runoff events with slope failure from those without slope failure, and identified the seasonal sediment source in the upper catchment, since there more slope failure runoff events occurred with higher sediment yield. The monitoring at the two sites also revealed the net sediment deposition between the two sites. A semi-distributed model, ArcSWAT2012, and a lumped model, the tank model, coupled with power function, were applied to simulate discharge and sediment load time series, obtained in 2011 to 2014. In ArcSWAT2012, the total basin area (62.47 km2) was divided into three sub-basins (subbasin 1, subbasin 2, subbasin 3), as sub-basins into hydrological response unit (HRU) based on elevation, soil type, land use and

slope classes that allow a high level of spatial detail simulation. In this study I have used the data of discharge, Q (m3/s), suspended sediment concentration (SSC; C, mg/L) and sediment load, L (kg/s) for non-frozen period of April 2011 to November 2014, weather data of 2008 to 2014, and soil data. Soil water content and groundwater storage in soil layers could change every year because the amounts of snowfall and snowmelt are different. So I have utilized my models at annual base. As a result, both SWAT and the tank model plus power function reasonably simulated daily mean discharge and sediment load time series. The simulations results indicate that most of the sediment input in this catchment originates in the western subbasin 2 and sediment deposition occurs between two sites; the same scenario was seen in observed monitoring data also. At present, the interpretation of the quantitative results of sediment load is not yet so satisfactory, because of lack of model parameterization at a local scale in the SWAT and tank model. These results from the fact that the information on hydrological structures of soil and bedrock and behaviors of surface flow or subsurface flow is not sufficient. Hence, studies on discharging and sediment-eroding processes on and below the catchment slope (slope hydrology and sedimentology) are essential to understand the sediment loading processes on catchment scale.

# Contents

# CHAPTER ONE

## INTRODUCTION

### Introduction

Exploring fluvial sedimentary processes on catchment scale is useful for studies on the forest management, material cycle and ecosystem of short time scale and topographic evolution of long scale. The fluvial transportation of sediment is also related to sedimentation, material cycle and ecosystem in coastal regions. Erosion and sedimentation processes decline soil fertility and decrease agricultural yields. It is important to know how sediment is yielded and fluvially loaded in a catchment with respect to the forest and land managements on small time scale of 1 to 100 years order and the landform development on large time scale of $10^3$ to $10^5$ years (**Baker, 1987**). The "slope failure" in the title of this paper is a phenomenon that a slope collapses abruptly due to weakened self-retain ability of the earth under the influence of a rainfall, snowmelt water or an earthquake. Slope failure includes bank collapse and landslide. Because of sudden collapse of slope, many people fail to escape from it if it occurs near a residential area, thus resulting in a higher rate of fatalities. Dynamic processes of landslide on the catchment slope have been investigated by many geologists, geomorphologists and geophysicists (e.g., **Zˆezere et al., 2005; Ashland & McDonald, 2010; Ekstrom & Stark 2013**). However, studies on subsequent fluvial sedimentation processes, connected to sediment load of river, are not enough (**Tsai et al., 2012**). The acquirement of discharge and suspended sediment concentration time series in a river allow us to explore the source location, availability and loading processes of sediment in the catchment **(Walling and Webb, 1982**; **Asselman**, **1999**) and to simulate long-term sediment yield or sediment load by modelling (**McCullough et al., 2008**; **Qiu et al., 2012**).

With respect to discharging processes in a catchment influenced by tectonic movement, groundwater flow systems in bedrocks with fractures or faults are investigated (**Michalski & Britton 1997**; **Banks & Robins 2002; Stamos et al. 2003; Seaton & Burbey 2005**). Neogene sedimentary rock as in the Oikamanai River catchment tends to have high frequency of landslide, compared with metamorphic rock, Mesozoic and Paleozoic rocks and volcanic rocks (**Araiba et al. 2008**). It is because the Neogene sedimentary rock is relatively soft, and thus easily receives the weathering. In case of the Oikamanai River catchment, Neogene sedimentary rock is also accompanied by active faults. These focus on the hydrological role of fractures or faults in groundwater flow system. Several adverse economic and environmental impacts due to the damaging effects of soil erosion have been reported.

It has remained a challenge to estimate changes in sediment yield over time in a catchment owing to the complexity of the processes involved in the detachment and transport of fluvial sediment. Different approaches have been adopted for sediment yield estimation. The most reliable method for sediment load estimation is direct measurement at the catchment level. Sediment concentrations are usually measured infrequently because very frequent monitoring over the long term is costly. It has also been noted that a sediment sampling strategy should be designed to capture high sediment concentrations for long-term monitoring to provide better results (**Thomas, 1988**).

The applications of empirical models for estimating sediment load have shown promise. Estimation of sediment load is commonly achieved by establishing a sediment rating curve. Empirical rating curves describing relationships between sediment load and instantaneous water discharge are often used. Some researchers have suggested that an excellent sediment rating curve could be constructed using a limited set of data (**Gao, 2008**). Sediment rating curves are

useful in predicting sediment yield, but they are site specific and have limitations when it comes to interpreting erosion processes (landscape erosion and in-stream erosion/sedimentation). Distributed and process-based watershed models are capable of capturing these complex processes both spatially and temporally. This category of models can be used to provide an enhanced understanding of the relationship between hydrologic processes, landforms, land management, soil factors and erosion/sedimentation (**Van Rompaey et al., 2001; Easton et al., 2010**). Each of many model parameters has a physical meaning, but all of them cannot be measured directly in the field, and therefore model validation can be concluded on the basis of a short field survey and short time series of meteorological and hydrological data. Various hydrological models have been proposed to predict sediment yield and sediment load in a catchment, such as the European Soil Erosion Model (EUROSEM) (**Morgan et al., 1998**), the Water Erosion Prediction Project (WEPP) (**Nearing et al., 1989**) and the Soil and Water Assessment Tool (SWAT), etc. (**Neitsch et al.,2005, Merritt et al., 2003; Aksoy and Kavvas, 2005; Talebizadeh et al., 2010**). However, behaviors of subsurface or surface flow on the hillslope in a forested catchment, accompanied by sediment erosion and transport, are still unknown. There are few studies about sediment-loading processes on catchment scale.

In this study, characteristics of river-suspended sediment load in the Oikamanai River catchment, accompanied by slope failure, are depicted from hourly time series of discharge, suspended sediment concentration (SSC) and sediment load, and sediment loading processes in the catchment are proposed by incorporating simulations of discharge and sediment load by field observations and modeling.

Here, I have focused on extra sediment supply to the river channel by bank collapse or landslide by using observed data, and applied a semi-distributed model, Soil Water Assessment

Tool (SWAT) and a lumped model, the tank model to time series of daily mean discharge and sediment load in the river basin to find the sediment sources and sediment loading process of the forested Oikamani River catchment influenced by slope failure.

# CHAPTER TWO

## STUDY AREA AND METHODS

### 2.1. Study area

The Oikamanai River is a main influent river of the Oikamanai Lagoon opening sporadically to the Pacific Ocean in the Tokachi coastal region of southeastern Hokkaido, Japan (**Fig. 2.1; Chikita et al., 2012, 2015**). The river catchment (42°33'46" to 42°40'40"N, 143°21'47" to 143°28'36"E; altitude, 6 m to 330 m asl) upstream of site R1 has the area of 62.47 km$^2$, the mean slope angle of 17° and the mean riverbed gradient of 0.033 (**Fig. 2.1; Hossain et al., 2015**). The digital elevation model (DEM) in **Figure2.1** is made up by 0.1 km × 0.1 km mesh. The distribution of slope angle corresponds to that of the surface geology (**Fig. 2.2**); the upper,

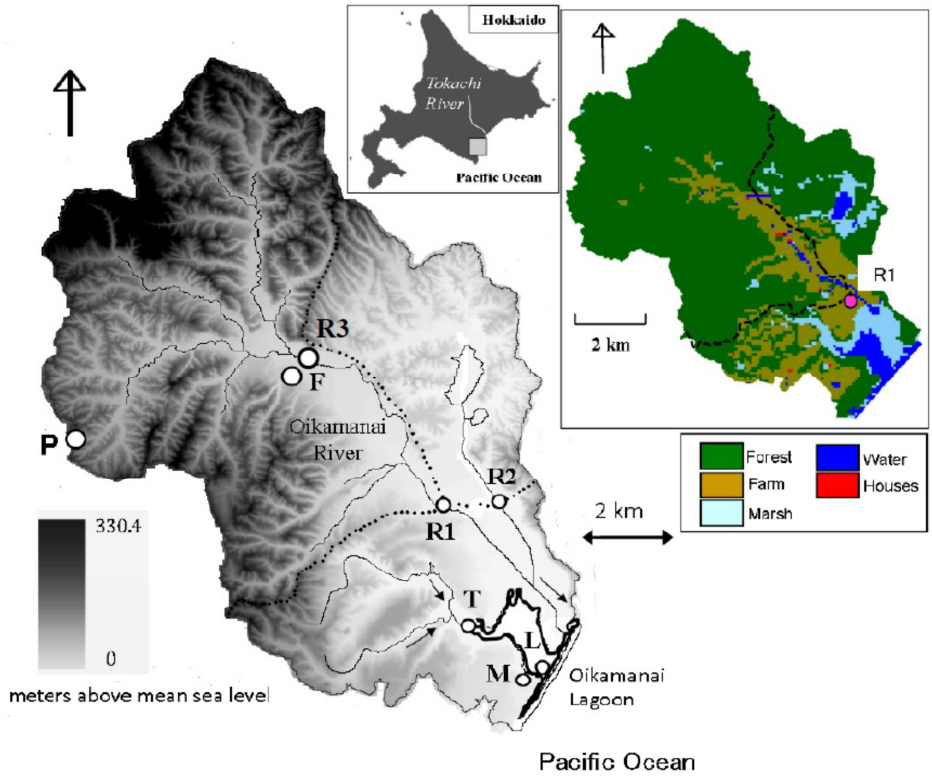


**Fig. 2.1** Location of the Oikamanai River catchment in eastern Hokkaido, Japan, and observation sites in the catchment, shown by the digital elevation model (DEM). The land use map is also shown (right).

middle and lower regions with relatively steep slope in the northwest to southeast directions are occupied by sedimentary rocks of early to middle Miocene, middle to late Miocene and late Miocene to Pliocene, respectively, and the lowest region with relatively gentle slope just upstream of site R1 by alluvial flood deposits. The sedimentary rocks are composed of conglomerate, sandstone, mudstone, siltstone and tuff. Neogene sedimentary rock as in the Oikamanai River catchment tends to have high frequency of landslide, compared with metamorphic rock, Mesozoic and Paleozoic rocks and volcanic rocks (**Araiba et al., 2008**). It is because the Neogene sedimentary rock is relatively soft, and thus easily receives the weathering. The sedimentary rocks in the mountainous regions are accompanied by many faults, which are due to the orogenic movement of the Hidaka Range at ca. 45 km southwest of the catchment. The northern faults are currently active, producing the high sediment yield from landslide or collapse

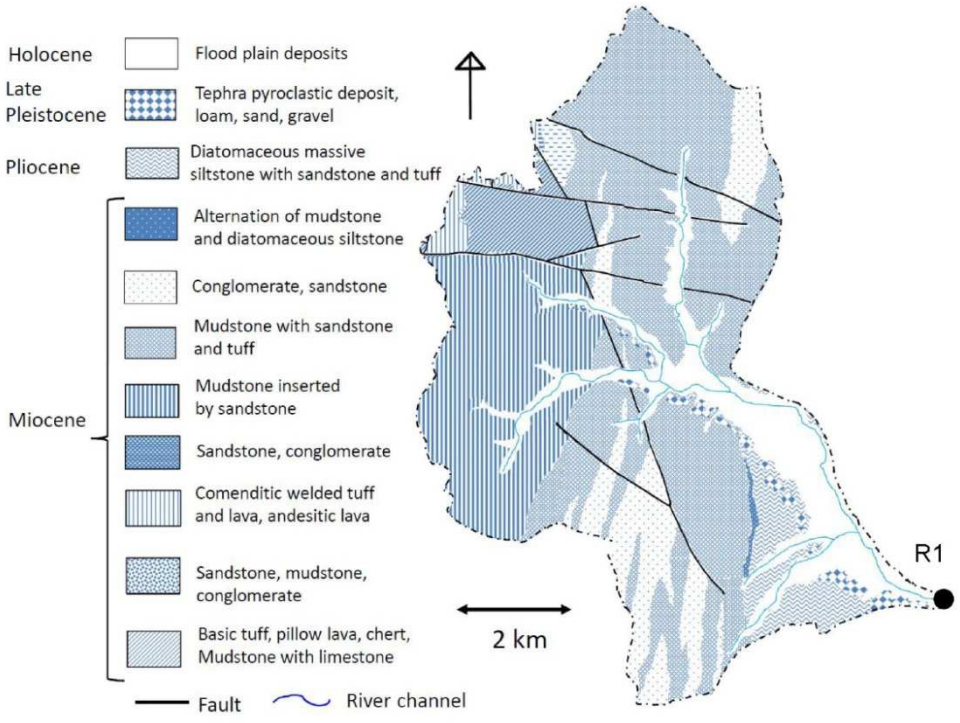


**Fig. 2.2** Geology of the catchment upstream of site R1

in the mountainous region (Tokachi Subprefecture HP; URL, http://www.tokachi.pref.hokkaido.lg.jp/sr/srs/gaiyou/sugata/sugata.htm) (**Fig. 2.2**). Sandy pyroclastic deposits of late Pleistocene are distributed on the catchment slope, connected to the area along the border of flood plain and forest regions. Such permeable deposits could make the seepage easy from the forest region to the flood plain. According to the Hjulström curve, such sandy deposits are easily eroded by overland flow or river flow. The catchment upstream of site R1 is covered by 88.3 % forest in the mountainous region, 10.6 % farmland (mostly, grassland) on the lowest alluvial plain and others. The forest is composed of ca. 50% broad-leaved and ca. 50% coniferous (mainly, Sakhalin fir; *Abies sachalinensis*) trees.

### 2.2. Methods

The monitoring of water level, air temperature, water temperature and water turbidity at site R1 was performed at 1 hour intervals by HOBO air pressure and water pressure loggers with temperature sensors (Onset Computer, Inc., USA; the range of 69 – 207 kPa and the accuracy of ±0.62 kPa for pressure, and the range of -20 to 50 °C and the accuracy of ±0.2 °C for temperature), and a self-recording turbidimeter of infrared back-scattering type with a window-cleaning wiper (type ATU3-8M, Advantech, Inc., Japan, with a range of 0 - 20,000 ppm and an accuracy of ±20 ppm), respectively, in April 2011 to November 2012. Instantaneous turbidity (ppm) was measured ten times at 1 sec interval every 1 hour signal and averaged for the 10 samplings. The averaged turbidity was converted into suspended sediment concentration (SSC; mg $L^{-1}$) from simultaneous water samplings by a depth-integrating sampler (**Fig. 2.3**). Two regression lines with a boundary at 200 ppm were acquired, since relations between electric signal and turbidity are obtained at 0 – 200 ppm and 200 – 20,000 ppm in manufacture, using

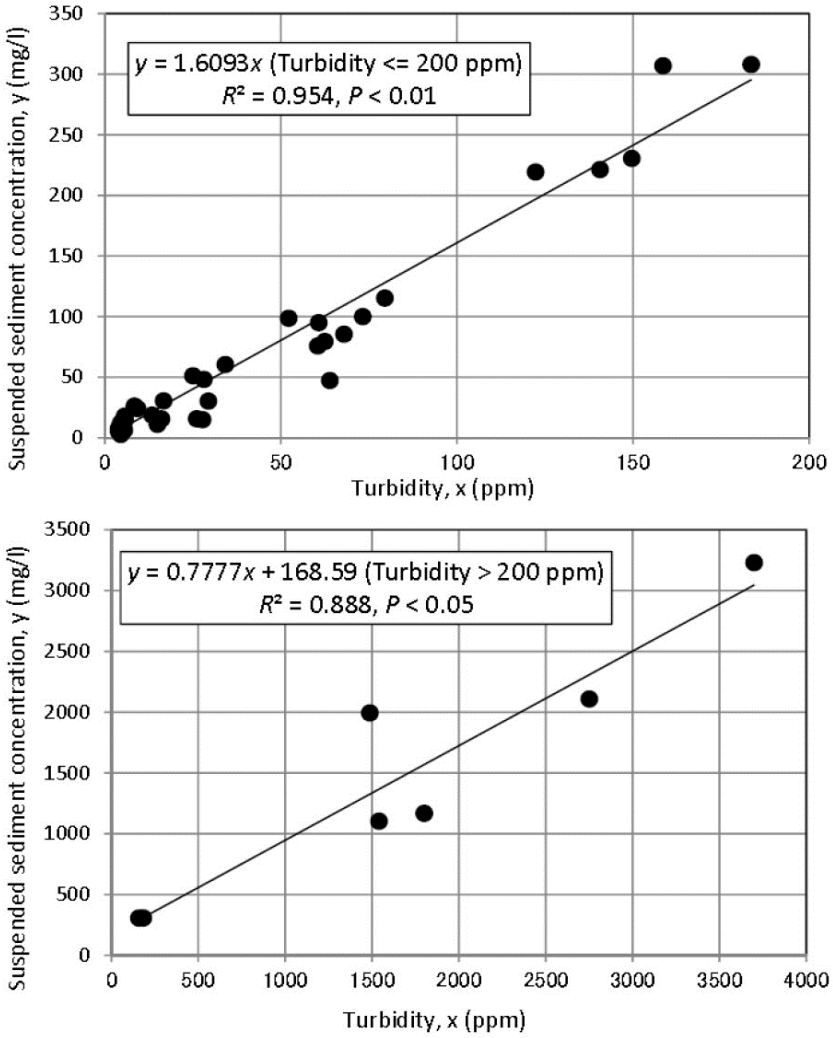


**Fig. 2.3** Relationships between water turbidity (ppm) and suspended sediment concentration (SSC: mg/L), separated by turbidity of 200 ppm.

suspension of kaolin powder. Water level, $h$ (m), at site R1 was changed into river discharge, $Q$ ($m^3$ $s^{-1}$), by the $h$ - $Q$ rating curves $Q=7.740\cdot(h+0.1507)^2$, $R^2$ = 0.935, in 2011-2012, $Q=13.57\cdot(h+0.077)^2$ at $h \leq 0.869$ m, $R^2$ = 0.995 & $Q=3.865\cdot(h+0.809)^2$ at $h > 0.869$ m, $R^2$ = 0.999 in 2013, $Q=24.38\cdot h^{4.77}$ at $h \leq 0.8$ m, $R^2$ = 0.906 & $Q=3.977\cdot(h+0.738)^2$ at $h > 0.8$ m, $R^2$ = 0.998 in 2014 and at site R3 by $Q=17.90\cdot h^{1.90}$ at $h \leq 0.15$ m, $R^2$ = 0.951 & $Q=11.18\cdot h$ -1.253 at $h > 0.15$ m, $R^2$ = 0.961 which were obtained by measuring discharge several times per year

and applying the Manning equation to the channel cross-section at site R1 and R3. The route of the Oikamanai River channel is artificially regulated by concrete blocks constructed in 1996. However, riverbed configuration could change to a degree by sediment deposition or erosion in the river channel. The *h* - *Q* rating curves is thus applicable only in 2011 -2014. The sediment load, *L* (kg $s^{-1}$), was calculated by $L = C \times Q$, where *C* is suspended sediment concentration (g $L^{-1}$).

The weather data were obtained at site M (rainfall and air temperature) near the Oikamanai Lagoon (**Chikita et al., 2012, 2015**) at 4.0 km south-southeast of site R1, and at two weather stations at the Taiki Aerospace Research Field (rainfall, air temperature, solar radiation, and wind speed and direction) 9.6 km south of site R1 and Taiki town (snow depth, rainfall, air temperature, and wind speed and direction) 18.9 km southwest of site R1. The distinction between rainfall and snowfall in the catchment was performed under air temperature more than 0 °C at site M (altitude, 6 m asl).

As preparation for simulating discharge and sediment load time series, actual evapotranspiration in the catchment was estimated by the one-layer model (**Kondo, 1998**; **Hossain et al., 2015**), and elevation effects on air temperature and rainfall were considered. Considering a topographic effect on the solar radiation, the DEM in **Figure 2.1** was applied to know the slope angle and aspect of the basin. The elevation effect on rainfall was explored by using rainfall data at site M, site F and site P, and analytical rainfall data of 1 km × 1 km mesh by the Japan Meteorological Agency. The mesh data are built up at 1 h intervals by coupling *in situ* rainfall with radar echo, and the mesh covers main Japanese islands (Hokkaido, Honshu, Shikoku, Kyushu, etc.) (URL: http://www.jma.go.jp/jma/jma-eng/jma-center/nwp/outline2013-nwp/index.htm).

### 2.3 Grain size analysis

Grain size is very important factor for discharge and sediment loading processes. **Table 1** shows experimental results of hydraulic conductivity and grain size for the slope soils at site F. The forest soil at site F is relatively permeable at a depth of 0 - 20 cm at $K_s$ = 3.6×10$^{-3}$ cm s$^{-1}$. The $K_s$ value corresponds to the infiltration capacity of 13 mm h$^{-1}$, of which heavy rainfalls were never recorded in 2011 - 2014. Meanwhile, the forest soil is most permeable at depths of 30 – 40 cm, indicating the high hydraulic conductivity of $K_s$ = 1.7 × 10$^{-2}$ cm s$^{-1}$. The high hydraulic conductivity is due to the inclusion of gravels, although the percentage of silt and clay is similar to that in the lower much less permeable layer ($K_s$ = 1.8×10$^{-5}$ cm s$^{-1}$ at 40 – 50 cm depth). The gravels probably originate in tephra pyroclastic deposits from volcanic eruptions in the Holocene. Thus, the downslope subsurface flow could occur in the highly permeable layer during rainfall or snowmelt, because the vertical percolation is interrupted by the much less permeable soil layer at 40 – 50 cm depth. The grassland soil is impermeable except for the sandy layer of 0 – 20 cm at $K_s$ = 1.4×10$^{-3}$ cm s$^{-1}$, which is equivalent to the infiltration capacity at 5.0 mm h$^{-1}$. The grassland on the flood plain between soil sampling site and site R1 could produce the subsurface flow only in the surficial soil layer, and, at rainfalls of more than 5.0 mm h$^{-1}$, also the Hortonian overland flow, of which the rainfalls occurred a few times in 2011- 2014 (**Table2**).

**Table 1** Grain size and hydraulic conductivity for forest and grassland soils at site near F

| | Soil depth (cm) | Mean (μm) | Standard dev. (μm) | Gravel (%) | Sand (%) | Silt (%) | Clay (%) | Hydraulic Conductivity $K_s$ (cm s$^{-1}$) |
|---|---|---|---|---|---|---|---|---|
| Forest | 0 - 20 | 140.60 | 222.20 | 0.00 | 45.52 | 33.58 | 20.90 | 3.6x10$^{-3}$ |
| | 20 - 30 | 260.20 | 344.20 | 0.81 | 76.94 | 12.43 | 9.82 | 4.4x10$^{-3}$ |
| | 30 - 40 | 165.60 | 634.70 | 3.55 | 14.65 | 29.17 | 52.64 | 1.7x10$^{-2}$ |
| | 40 - 50 | 64.70 | 169.80 | 0.00 | 19.43 | 29.12 | 51.45 | 1.8x10$^{-5}$ |
| Grassland | 0 -20 | 113.70 | 172.50 | 0.00 | 40.92 | 29.29 | 30.80 | 1.4x10$^{-3}$ |
| | 20 - 47 | 59.90 | 124.30 | 0.00 | 23.53 | 33.44 | 45.47 | 6.4x10$^{-6}$ |
| | 47 - 59 | 45.00 | 101.70 | 0.00 | 19.73 | 26.31 | 55.49 | 6.7x10$^{-5}$ |

## 2.4 Observational results and discussion

**Figure 2.4** shows hourly time series of discharge, suspended sediment concentration (SSC), suspended sediment load and water temperature at site R1, air temperature and precipitation at the Aerospace Research Field, and snow depth at Taiki town in April 2011 to November 2014. As shown by water temperature at ca. 0 °C, the Oikamanai River was frozen down to the depth of the pressure logger for mid-December to March of every year. The rating curves were then not applicable at site R1 and R3, because the covered-ice growth and snow accumulation on the ice substantially increase the water pressure recorded. As a result, the accurate observation of

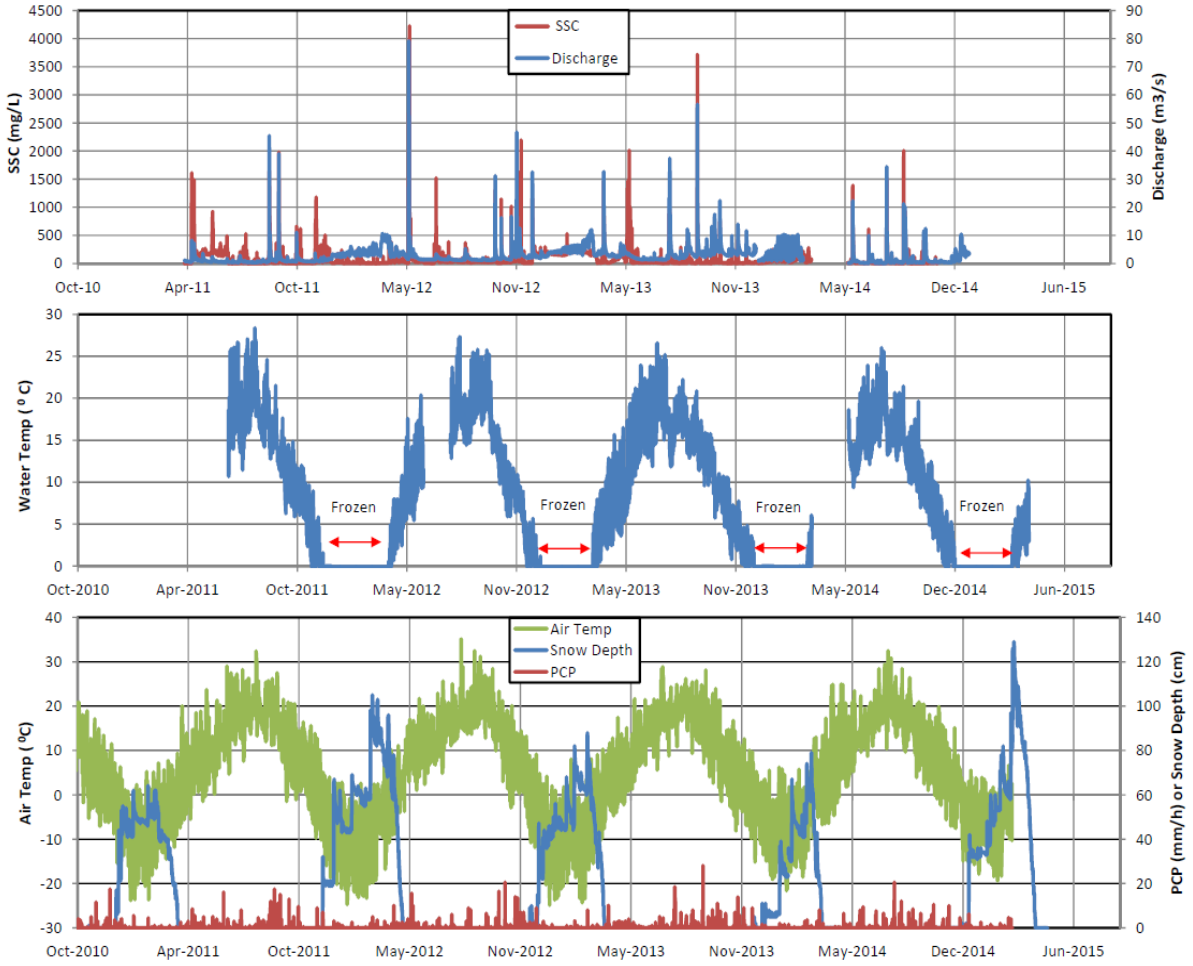


**Fig. 2.4** Hourly time series of discharge and water temperature at site R1, air temperature and precipitation at the Taiki Aerospace Research Field, and snow depth at Taiki town.

**Table 2** River runoff events with maximum discharge of more than 2 $m^3 s^{-1}$ observed in 2011 - 2013 and 1.4 $m^3 s^{-1}$ observed in 2014

$Q$: Discharge $S$: Suspended sediment concentration $L$: Suspended sediment load

| No. | Time period of runoff event | Mean $Q$ ($m^3/s$) | Max $Q$ ($m^3/s$) | Mean $S$ (mg/L) | Max $S$ (mg/L) | Mean $L$ (kg/s) | Max $L$ (kg/s) | Total rainfall (mm) | Remark |
|---|---|---|---|---|---|---|---|---|---|
| | 2011 | | | | | | | | |
| 1 | 0000 h, 24 April - 0200 h, 25 April | 7.69 | 14.00 | 957.00 | 1610.00 | 6.70 | 13.10 | 71.5 | slope failure |
| 2 | 0800 h, 28 April - 2300 h, 28 April | 5.65 | 7.10 | 645.00 | 1480.00 | 3.80 | 10.40 | 47.0 | slope failure |
| 3 | 1400 h, 13 May - 0100 h, 14 May | 3.04 | 3.53 | 225.00 | 253.00 | 0.69 | 0.88 | 37.0 | |
| 4* | 0200 h, 29 May - 0100 h, 31 May | 1.84 | 2.34 | 492.00 | 915.00 | 0.97 | 1.86 | 40.5 | slope failure |
| 5 | 2100 h, 16 July - 0000 h, 18 July | 2.02 | 2.71 | 77.50 | 205.00 | 0.18 | 0.56 | 32.5 | |
| 6 | 2300 h, 4 Sep. - 1000 h, 5 Sep. | 1.85 | 2.54 | 118.00 | 228.00 | 0.24 | 0.55 | 18.0 | |
| 7 | 1300 h, 5 Sep. - 0900 h, 8 Sep. | 10.90 | 45.30 | 611.00 | 1640.00 | 10.30 | 68.20 | 21.0 | slope failure |
| 8 | 2000 h, 17 Sep. - 1300 h, 20 Sep. | 2.55 | 4.07 | 74.50 | 364.00 | 0.23 | 1.44 | 42.5 | |
| 9 | 0000 h, 22 Sep. - 0800 h, 23 Sep. | 12.90 | 38.30 | 817.00 | 1960.00 | 13.90 | 52.50 | 88.0 | slope failure |
| 10 | 0100 h, 24 Sep. - 0900 h, 24 Sep. | 3.09 | 3.29 | 106.00 | 112.00 | 0.33 | 0.37 | 12.0 | |
| 11 | 2100 h, 22 Oct. - 1500 h, 23 Oct. | 6.38 | 10.90 | 368.00 | 656.00 | 2.70 | 7.10 | 59.5 | |
| 12 | 0500 h, 24 Nov. - 1800 h, 26 Nov. | 1.47 | 3.65 | 465.00 | 1180.00 | 0.62 | 1.41 | 24.0 | slope failure |
| | 2012 | | | | | | | | |
| 13 | 0300 h, 4 May - 0200 h, 6 May | 33.30 | 79.00 | 1690.00 | 4220.00 | 58.20 | 211.00 | 221.0 | slope failure |
| 14 | 1500 h, 6 May - 2200 h, 7 May | 6.62 | 9.69 | 362.00 | 810.00 | 2.50 | 5.30 | 30.5 | |
| 15 | 1800 h, 11 May - 0300 h, 13 May | 4.30 | 5.17 | 128.00 | 209.00 | 0.57 | 1.10 | 32.0 | |
| 16 | 1900 h, 15 May - 0700 h, 17 May | 2.88 | 3.42 | 41.60 | 65.40 | 0.12 | 0.22 | 19.5 | |
| 17 | 1500 h, 20 June - 0100 h, 22 June | 2.86 | 3.40 | 463.00 | 1520.00 | 1.40 | 5.10 | 48.5 | |
| 18 | 0100 h, 10 Aug. - 1800 h, 12 Aug. | 3.33 | 5.20 | 151.00 | 368.00 | 0.56 | 1.84 | 44.5 | slope failure |
| 19 | 1500 h, 13 Aug. - 1100 h, 14 Aug. | 2.77 | 3.42 | 37.50 | 61.40 | 0.11 | 0.19 | 17.0 | |
| 20 | 0400 h, 1 Oct. - 0200 h, 2 Oct. | 11.70 | 31.20 | 499.00 | 1310.00 | 7.98 | 40.90 | 89.5 | |
| 21 | 1900 h, 11 Oct. - 1600 h, 12 Oct. | 6.63 | 16.26 | 415.00 | 1130.00 | 3.67 | 18.38 | 40.0 | |
| 22 | 0600 h, 29 Oct. - 2000 h, 29 Oct. | 9.34 | 16.65 | 421.00 | 1010.00 | 4.73 | 12.48 | 53.0 | |
| 23 | 2300 h, 1 Nov. - 1700 h, 3 Nov. | 5.05 | 7.75 | 157.00 | 382.00 | 0.86 | 2.73 | 42.0 | |
| 24 | 0900 h, 7 Nov. - 1800 h, 8 Nov. | 22.10 | 46.67 | 693.00 | 1030.00 | 17.60 | 42.97 | 77.0 | slope failure |
| 25 | 1400 h, 12 Nov. - 1300 h, 13 Nov. | 8.20 | 12.53 | 291.00 | 583.00 | 2.71 | 7.30 | 36.5 | |
| 26 | 1000 h, 14 Nov. - 1300 h, 15 Nov. | 5.32 | 5.83 | 642.60 | 2167.00 | 3.40 | 10.66 | 16.5 | slope failure |
| 27 | 2200 h, 28 Nov. - 2000 h, 29 Nov. | 2.70 | 3.00 | 21.50 | 46.60 | 0.06 | 0.13 | 9.5 | |
| 28 | 1400 h, 4 Dec. - 0500 h, 6 Dec. | 14.47 | 32.40 | 560.00 | 1150.00 | 10.20 | 36.20 | 75.5 | |
| | 2013 | | | | | | | | |
| 29 | 0600h, 7 Apr. - 0900h, 9 Apr. | 14.18 | 29.87 | 644.49 | 1465.18 | 11.70 | 43.47 | 86.5 | slope failure |
| 30 | 0800h, 6 May - 0600h, 8 May | 6.31 | 7.86 | 187.38 | 294.72 | 1.22 | 2.15 | 29.5 | |
| 31 | 2300h, 11 May - 0100h, 13 May | 5.88 | 7.38 | 156.39 | 251.33 | 0.96 | 1.68 | 24.5 | |
| 32* | 0300h, 29 July - 0300h, 3 Aug. | 13.24 | 34.44 | 379.27 | 962.53 | 7.22 | 31.12 | 188.5 | |
| 33 | 0300h, 30 Aug. - 1000h, 31 Aug. | 7.89 | 10.43 | 138.69 | 385.20 | 1.26 | 4.02 | 40.0 | |
| 34 | 2100h, 31 Aug. - 0000h, 2 Sept. | 8.85 | 9.77 | 119.19 | 175.25 | 1.08 | 1.71 | 28 | |
| 35 | 1500h, 16 Sept. - 1700h, 17 Sept. | 22.30 | 52.91 | 813.17 | 3712.48 | 23.78 | 137.16 | 115.5 | slope failure |
| 36 | 1400h, 25 Sept. - 1500h, 26 Sept. | 5.61 | 7.57 | 70.83 | 143.97 | 0.42 | 1.04 | 16.5 | |
| 37 | 1900h, 2 Oct. - 1900h, 3 Oct. | 3.11 | 7.44 | 168.49 | 503.89 | 0.59 | 2.78 | 20.0 | |
| 38 | 1200h, 9 Oct. - 0000h, 11 Oct. | 3.09 | 8.12 | 396.70 | 586.56 | 1.05 | 3.64 | 22.0 | slope failure |
| | 2014 | | | | | | | | |
| 39 | 1800 h, 12 Jun. -1800 h, 15 Jun. | 7.41 | 22.23 | 324.76 | 1386.46 | 4.24 | 30.83 | 48.0 | |
| 40 | 1800 h, 10 Jul. -1900 h, 11 Jul. | 4.09 | 9.89 | 246.63 | 610.83 | 1.44 | 5.96 | 19.5 | |
| 41 | 2200 h, 10 Aug. -1800 h, 12 Aug. | 11.37 | 34.38 | 467.89 | 1475.05 | 7.90 | 50.72 | 111.0 | |
| 42 | 1500 h, 19 Aug. -0900 h, 20 Aug. | 2.31 | 3.81 | 76.91 | 144.43 | 0.21 | 0.55 | 14.5 | |
| 43 | 0800 h, 9 Sep. -0600 h, 10 Sep. | 11.84 | 21.15 | 735.94 | 2006.83 | 11.00 | 42.08 | 3.0 | |
| 44 | 0300 h, 11 Sep. -1800 h, 13 Sep. | 11.49 | 20.27 | 370.70 | 935.13 | 5.27 | 18.96 | 53.0 | |
| 45 | 0700 h, 14 Oct. -1400 h, 15 Oct. | 6.57 | 11.53 | 169.04 | 406.74 | 1.52 | 4.56 | 37.5 | slope failure |
| 46 | 1000 h, 17 Oct. -0800 h, 19 Oct. | 5.99 | 12.41 | 105.66 | 523.24 | 0.96 | 6.50 | 15.5 | |
| 47 | 2000 h, 02 Nov. - 1400 h, 4 Nov. | 0.92 | 1.48 | 19.97 | 118.67 | 0.02 | 0.11 | 1.5 | slope failure |

* including continual two runoff events

snowmelt runoffs in the snowmelt season was difficult, because snowmelt water then flew on the covered ice. Hence, only rainfall river runoff events under ice- or snow-free condition are here discussed. Rainfall runoff events with maximum discharge of more than 2.0 $m^3$ $s^{-1}$ in 2011-2013 and more than 1.4 $m^3$ $s^{-1}$ in 2014 were observed 47 times at site R1 in April to November of 2011- 2014 (**Table 2**). The duration, *D* (h), of runoff were defined as time periods when both discharge and SSC start to increase and SSC becomes lowest after maximum discharge and SSC. The largest runoff event (no. 13 in **Table 2**) occurred by a heavy rainfall (totally, 221 mm; **Figure 2.4**). The peak discharge was 79.0 $m^3$ $s^{-1}$ at 1400 h on 4 May 2012, accompanied by suspended sediment concentration of 2,670 mg $L^{-1}$. However, the highest suspended sediment

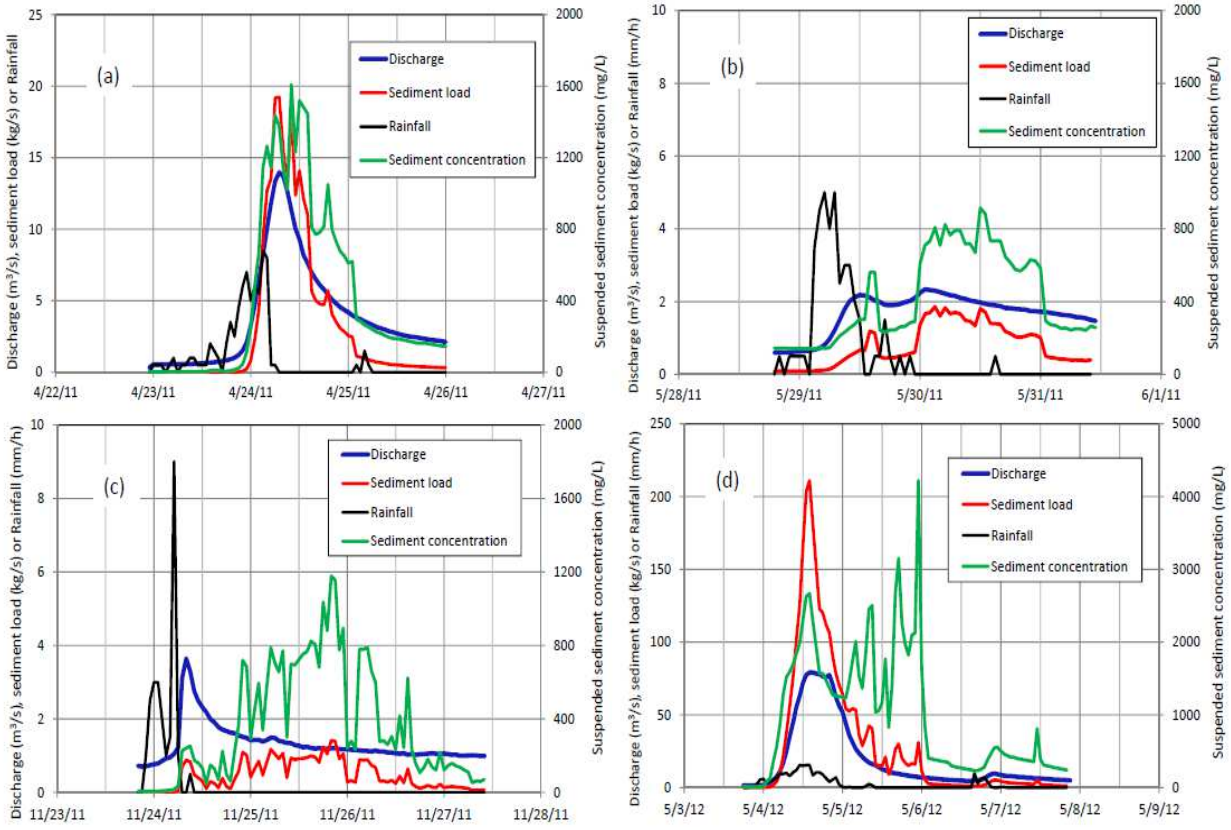


**Fig. 2.5** Hourly time series of discharge, SSC and sediment load at site R1, and rainfall at site P for river runoff events with extra sediment supply. (a) no. 1, (b) no. 4, (c) no. 12 and (d) no. 13 in Table 2.

concentration at 4,220 mg $L^{-1}$ was recorded at 2300 h on 5 May 2012 during declining discharge (7.4 $m^3$ $s^{-1}$) after rainfall (**Figure 2.5d**). This suggests that the extra sediment supply to the channel reach upstream of site R1 occurred by riverbank collapse or land slide on the surrounding slope. Of all the runoff events, fifteen runoff events (Event no. 1, 2, 4, 7, 9, 12, 13, 18, 24, 26, 29, 35, 38, 45 and 47 in **Table 2**) exhibited an increase in SSC after maximum discharge or corresponding maximum SSC. **Figure 2.5** shows time series of hourly rainfall, discharge, SSC and sediment load for events of (a) no. 1, (b) no. 4, (c) no. 12 and (d) no. 13, accompanied by the extra sediment supply. There are two types for the extra sediment supply; (1) SSC increases until maximum discharge appears, but subsequently higher SSC continues for more than half a day (**Figure 2.5b, 2.5c and 2.5d**). (2) SSC is peaked at or around the maximum discharge and then abruptly decreases within about half a day (**Figure 2.5a**). In nos. 4 and 12 events (**Figure 2.5b and 2.5c**), the temporal variation of sediment load after maximum discharge is influenced by SSC rather than discharge, since discharge is then relatively stable. Examples of runoff events without extra sediment supply are shown in **Figure 2.6**. Any increase in SSC after maximum discharge does not appears in the four events. There is a time difference of 0 – 2 h between peak discharge and peak SSC. The bank collapse and land slide could be induced from gravitational instability of bank sediment and surrounding slope soil and bedrock, respectively, which is due to an increase in water storage by rainfall and the production of slip plane. However, it is unknown in detail how such slope failure produces the extra sediment supply to a river channel, since there have been few observations of the fluvial sedimentary processes in the upstream.

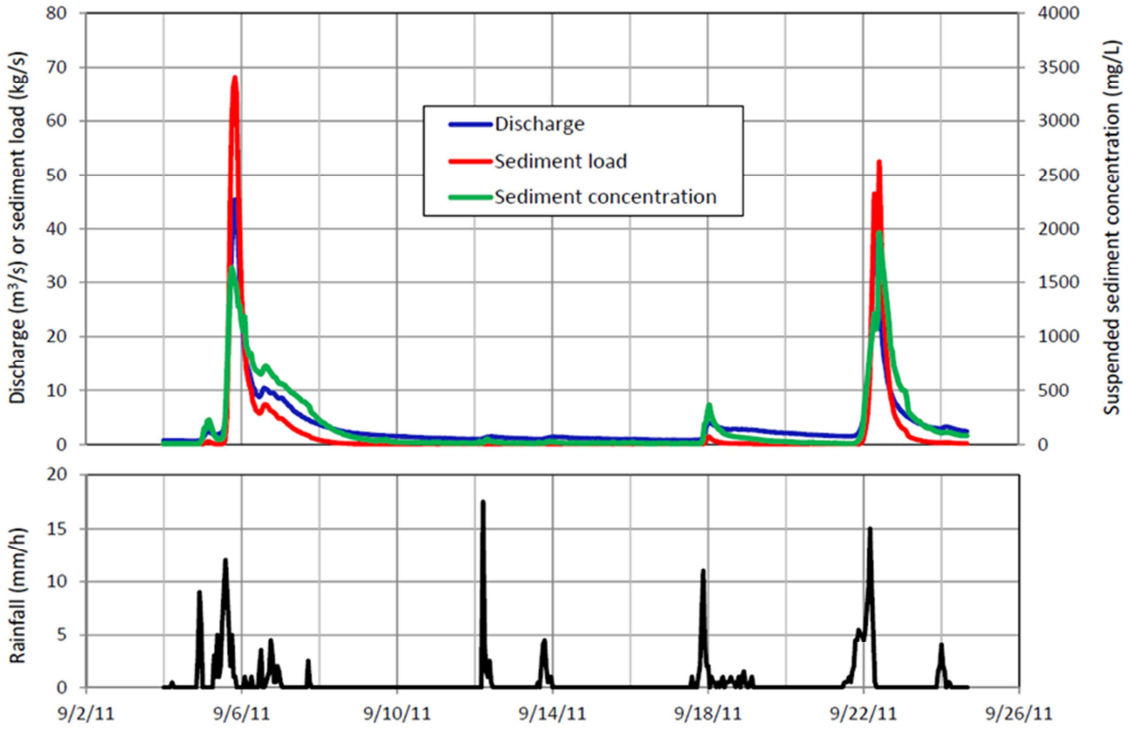


**Fig. 2.6** Hourly time series of discharge, SSC and sediment load at site R1, and rainfall at site P for river runoff events without extra sediment supply.

**Figure 2.7** shows relations between the total runoff rate $R_d$ (mm) and total sediment yield $S_d$ (g m$^2$) for all the runoff events in 2011-2014 at site R1. $R_d$ and $S_d$ were calculated as $R_d = 24 \cdot 1000 \cdot R \cdot D^{-1} \cdot A^{-1}$ and $S_d = 24 \cdot 1000 \cdot S \cdot D^{-1} \cdot A^{-1}$, where $R$ is total discharge (m$^3$) for the event duration $D$ (h), $A$ is catchment area (m$^2$) and $S$ is total sediment load (g) for duration $D$(h). Though there are only fifteen plots for runoff events with extra sediment supply (white circles in **Figure 2.7**), they seem to exhibit sediment yield about 2.8 times more than that for the events without extra sediment supply (black circles in **Figure 2.7**), as shown by the magnitude of the slope for the two regression lines. At $R_d$ < ~ 12 mm, however, the $R_d$ – $S_d$ relations are very similar, reflecting similar variations of discharge and sediment load for the events with or without extra sediment supply (**Figure 2.5 and 2.6**).

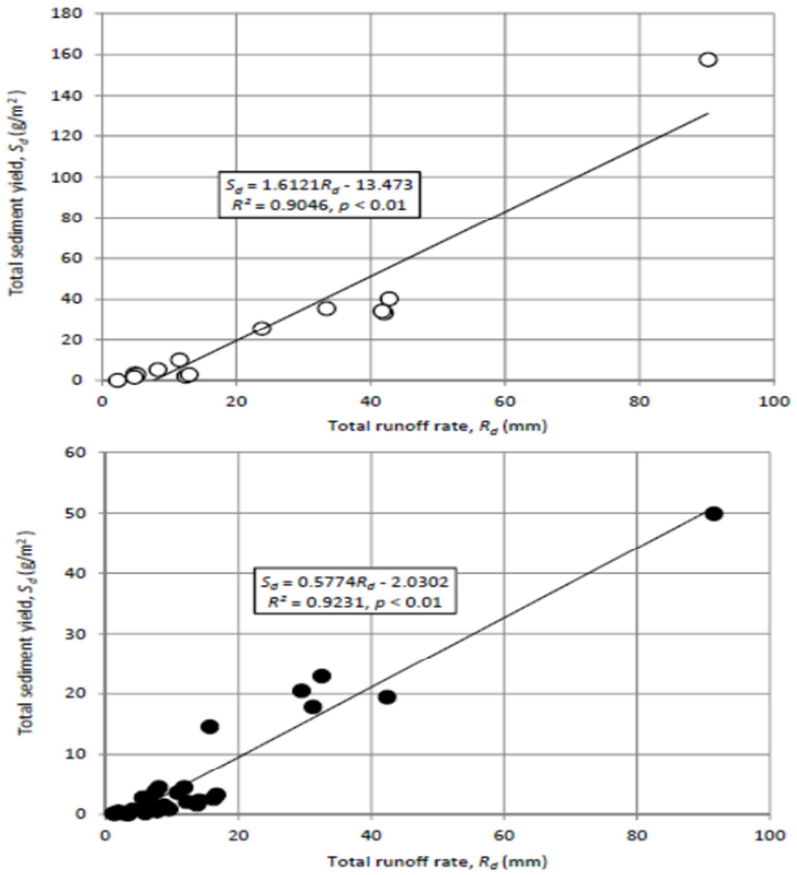


**Fig. 2.7** Relations between total runoff rate $R_d$ (mm) and total sediment yield $S_d$ (g m$^{-2}$) for rainfall runoff events with (white circles) and without (black circles) extra sediment supply at site R1.

# CHAPTER THREE

## MODELLING

### 3.1 Background

Rainfall and surface runoff erodes surface soil and sediment transported from the land surface to stream networks are reasonable for reservoir sedimentation and aquatic habitant degradation (**Haag et al., 2001; Boithias et al., 2011, 2013; Kerr et al., 2011; Cerro et al., 2013, 2014**). Several adverse economic and environmental impacts due to the damaging effects of soil erosion have been reported. The on-site effect of soil erosion in terms of declining soil fertility and decreased agricultural yields are well known around the world. Environmental consequences are primarily off-site effects due to the pollution of natural waters (**Lal, 1998**). Understanding the dynamics of sediment transfer from land to watercourses and quantifying sediment yields are essential for controlling land soil erosion and implementing appropriate mitigation practices to reduce stream sediment and associated pollutant loads, and hence improve surface water quality downstream (**Heathwaite et al., 2005**). Downstream erosion and sedimentation implications are of increasing interest for catchment management, such as the design of dam reservoirs, river restoration, and the design of stable channels. It has remained a challenge to estimate changes in sediment yield over time in a catchment owing to the complexity of the processes involved in the detachment and transport of fluvial sediment. Different approaches have been adopted for sediment yield estimation. The most reliable method for sediment load estimation is direct measurement at the catchment level. Sediment concentrations are usually measured infrequently because very frequent monitoring over the long term is costly. It has also been noted that a sediment sampling strategy should be designed to

capture high sediment concentrations for long term monitoring to provide better results (**Thomas, 1988**).

Direct field measurements of discharge, turbidity and soil sampling have been used to quantify local erosion and sediment loading in streams but these are difficult to relate to whole watershed processes. Alternatively, sediment load dynamics can be estimated remotely using models of erosion processes at varied spatial scales. The increasing availability and use of basic landscape measures in a Geographic Information System (GIS) have led to the development of a variety of GIS-based erosion and sediment load modeling approaches. Many of these models are based on equations for calculating soil erosion, such as the Universal Soil Loss Equation (USLE) and its revised versions, Revised USLE (RUSLE) and Modified USLE (MUSLE). The USLE estimates average soil loss over time as a product of five factors: rainfall erosivity index, soil erodibility, slope length and steepness, land cover management, and support practice factor. These factors can be computed in a GIS using widely available spatial data such as climate, soil, geology, topography, hydrology, land use, and land cover data. Although USLE was designed for, and used most widely, in estimating erosion from agricultural lands, efforts to modify USLE for use in watersheds that are more topographically complex and with a higher diversity of land uses have led to the development of erosion models such as the Automated Geospatial Watershed Assessment (AGWA) and the RUSLE model. Some models not only calculate soil erosion, but they also simulate the transport of eroding soil down hillslopes and into stream channels by incorporating hydrological modeling, such as the Soil and Water Assessment Tool (SWAT). For estimating discharge, sediment load the empirical models have shown very important role. The empirical models save our time, economy and there is some parameter which is little bit tough to measure directly but by modeling we can easily measure those parameters.

Discharge and sediment load are estimated by establishing discharge and sediment rating curves from frequent discharge measurements and application of Manning's equation to the channel cross-section by topographic survey. In the absence of actual suspended sediment concentration (SSC) measurements, hydrologists have used sediment rating (sediment transport) curves to estimate (predict) SSC for subsequent discharge calculations. Sediment rating curves are useful in predicting sediment yield, but they are site specific and have limitations when it comes to interpreting erosion processes (landscape erosion and in-stream erosion/sedimentation). Different modeling approaches have been developed to predict erosion and sediment delivery to streams based on landscape features that incorporate land use disturbance, topography, geology, and climate.

Hydrological models are among the available tools used to forecast and predict the quantity and quality of water, sediment load for decision makers (**Chow et al., 1988**). Some of these models could also predict the impacts of natural and anthropogenic changes on water resources and also to quantify the spatial and temporal availability of the resources. However, the challenges lie in choosing and utilizing these models for a specific basin and managerial plan.

### 3.2 Tank Model

The tank model is a simple model, composed of three or four tanks laid vertically in series as shown in **Figure. 3.1**. Precipitation is put into the top tank, and evaporation is subtracted from the top tank. If there is no water in the top tank, evaporation is subtracted from the second tank; if there is no water in both the top and the second tank, evaporation is subtracted from the third tank; and so on. The outputs from the side outlets are the calculated runoffs. The side output from the top tank is considered as surface flow, output from the second tank as

intermediate flow and output from the third or lowest tank as baseflow. The bottom output from the first and second tank is considered as percolation and from the third or lowest tank as leakage to other catchment. In tank model sediment erosion and transported by surface flow and river flow using power function.

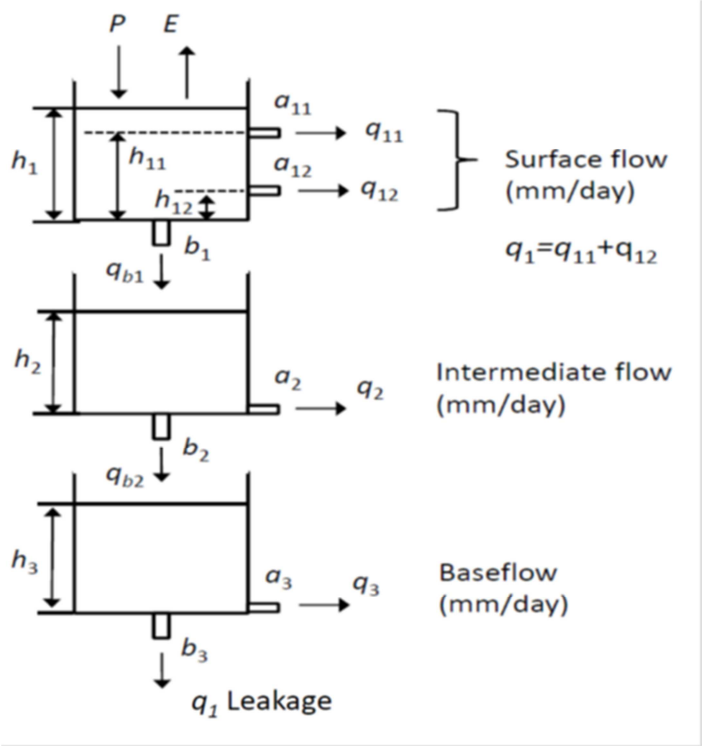


**Fig. 3.1** Tank layout for the tank model

In order to clarify what works as sediment-loading agents and to estimate their contribution to total sediment load in the Oikamanai River catchment, the discharge and sediment load time series at site R1 (**Figure 2.4**) are simulated by coupling the lumped tank model (**Sugawara, 1972**) with power function of discharge. For preparation, estimating evapotranspiration from the catchment and specifying a rainfall distribution in the catchment are needed. Daily mean discharge and sediment load data are utilized for simulation, because the evapotranspiration calculated is on a daily basis.

### 3.3 Estimate of evapotranspiration and rainfall on catchment scale

Daily evapotranspiration in the rainfall seasons in 2011-2014 was estimated by applying the one-layer model for forest and grassland (**Hossain et al., 2015**). First, the DEM and land-use maps of the catchment in **Figure 2.1** were utilized for the evapotranspiration calculation, because the effects of slope angle, slope aspect and surface condition on solar radiation should be considered. As a result, the averaged slope angle and aspect were 34.66° and 176.6° (clockwise from north at 0°), respectively. The basin slope thus faces almost south on average. With respect to land use, each value of albedo $\alpha$ and dimensionless bulk transfer coefficient of sensible heat $C_H$ was considered for forest and grassland separately. In the one-layer model, the leaf-surface temperature, $T_e$ (K), at a certain height in forest or grassland is obtained by the successive approximation method to satisfy the following heat balance equations:

$$(1-\alpha)K_\theta\downarrow + L\downarrow - G = \sigma T_e^4 + Q_H + Q_E \qquad (3.1)$$

$$Q_H = c_p\rho_a C_H U_z(T_e - T_z) \qquad (3.2)$$

$$Q_E = \lambda\cdot(\rho_a\,\varepsilon/p)\cdot\beta C_H\,U_z\{e_0(T_e) - e_z\} \qquad (3.3)$$

where $K_\theta\downarrow$ is the downward shortwave radiation (W m$^{-2}$) onto the catchment of slope angle $\theta$, $\alpha$ is the albedo, $L\downarrow$ is the downward longwave radiation (W m$^{-2}$), $G$ is the soil heat flux (W m$^{-2}$), $\sigma$ is the Stefan-Bolzmann constant (=5.670×10$^{-8}$ W m$^{-2}$ K$^{-4}$), $Q_H$ is the sensible heat flux (W m$^{-2}$), $Q_E$ is the latent heat flux (W m$^{-2}$), $\lambda$ is the vaporization heat (J kg$^{-1}$), $c_p$ is the specific heat (J kg$^{-1}$ K$^{-1}$) of water at constant pressure, $\rho_a$ is the air density ($\sim$1.2 kg m$^{-3}$), $\varepsilon$ is the ratio of water vapor density to dry air density (=0.622), $C_H$ is the dimensionless bulk transfer coefficient for the sensible heat flux, $T_z$ is the air temperature (K) at z, $u_z$ is the wind speed (m s$^{-1}$) at the height, $z$,

above the earth surface, $p$ is the air pressure (Pa) at $z$, $e_z$ is the vapor pressure (Pa) at $z$, $e_0(T_e)$ is the saturated vapor pressure (hPa) at the leaf-surface temperature $T_e$, and $\beta$ is the evaporation efficiency (=$C_E/C_H$; $C_E$, dimensionless bulk transfer coefficient for the latent heat flux).

Here, the albedo $\alpha$ is supposed to be constant at 0.10 or 0.15 for the forested (88.3% area) Oikamanai River catchment, since $\alpha$ = 0.05 – 0.15 for broadleaf forest, $\alpha$ = 0.1 – 0.2 for needleleaf forest and $\alpha$ = 0.15 – 0.25 for grassland (**Figure 2.1**: **Campbell & Norman 1998**). Actually, considering these ranges and the ratio of the land use area in **Figure 2.1**, the $\alpha$ value can be 0.08 - 0.18. The evaporation efficiency $\beta$ is given at 0.3 for Equations (3) and (4), because $\beta$ = 0.26 at the mixed broadleaf and needleleaf forest in summer (**Kondo, 1998**). When rainfalls at site M and site P was more than 40 mm $d^{-1}$, and relative humidity at site F was 100 %, $\beta$=1 was given. The bulk transfer coefficient, $C_H$, for the sensible heat flux is assumed to range from 0.005 to 0.008 for forest and grassland. Downward shortwave radiation $K_\theta\downarrow$ onto the basin slope is calculated by the following equations (**Tanaka et al., 2006**):

$$K_\theta\downarrow = K_d\cos i + K_s\cos^2\frac{\theta}{2} + \frac{1-\cos\theta}{2}\alpha K\downarrow \qquad (3.4)$$

$$\cos i = \cos\theta\sin h + \sin\theta\cos h\cos(A_s - A) \qquad (3.5)$$

where $K_d$ is direct shortwave radiation onto the normal surface, $K_s$ is scattered shortwave radiation onto the plane, $K\downarrow = K_d \sin h + K_s$, $i$ is an incident angle of shortwave radiation onto slope, $h$ is solar elevation, $A_s$ is solar azimuth, and $A$ is slope aspect (clockwise from $A$=0° for south-facing slope). $K_d$ and $K_s$ in Equation (3.4) were obtained by the following equations.

$$K_d = J_0 \, \xi^{1/\sin h} \tag{3.6}$$

$$K_s = \frac{1}{2} J_0 \sin h \frac{1-\xi^{1/\sin h}}{1-1.4\ln \xi} \tag{3.7}$$

where $J_0$ is solar constant (=1,353 W m$^{-2}$ as the annual average), $\xi$ is atmospheric transmissivity, and here is assumed to be 0.7 at constant. The downward shortwave radiation $K_\theta \downarrow$ onto the basin slope was calculated by using hourly $K \downarrow$ data ($\theta = 0°$) at the Taiki Aerospace Research Field. Here, $K_\theta \downarrow$ in Equation (3.4) was calculated at $\theta$ = 34.66° (averaged catchment slope) and $A$ = 356.6° (averaged slope aspect).

Daily mean values ($L_d \downarrow$) of the downward longwave radiation $L \downarrow$ in Equation (3.1) were calculated by the following equations (**Kondo, 1998**):

$$L_d \downarrow = \sigma T^4 \left[ 1 - \left( 1 - \frac{L_{df} \downarrow}{\sigma T^4} \right) C \right] \tag{3.8}$$

$$C = \frac{1 - \left( L_d \downarrow / \sigma T^4 \right)}{1 - \left( L_{df} \downarrow / \sigma T^4 \right)} \tag{3.9}$$

$$C = 0.03B^3 - 0.30B^2 + 1.25B - 0.04 \qquad (B \geq 0.0323) \tag{3.10}$$

$$C = 0 \qquad (B < 0.0323) \tag{3.11}$$

where $B = K_d \downarrow / K_{df} \downarrow$ ($K_d \downarrow$ and $K_{df} \downarrow$, daily mean shortwave radiation on the plane with cloud and in fair weather, respectively), $L_{df} \downarrow$ is daily mean longwave radiation in fair weather, and $T$ is daily mean air temperature (K) at z. $C$ is a factor of cloud effect with $C$=1 in fair weather. $L_{df} \downarrow$ is calculated as follows:

$$L_{df}\downarrow = \left(0.74 + 0.19x + 0.07x^2\right)\sigma T^4 \qquad (3.12)$$

$$x = \log w = 0.0315T_{dew} - 0.1836 \qquad (3.13)$$

where $w$ is total amount (cm) of effective water vapor, and $T_{dew}$ is daily mean dew point temperature (°C) at $z$, respectively. Daily mean shortwave radiation $K_{df}\downarrow$ in fair weather is calculated by using a relation with daily mean downward shortwave radiation $K_{0d}\downarrow$ on a horizontal surface in the upper end of atmosphere (**Kondo, 1998**).

When Equations (3.1) – (3.3) are applied at the daily base, the soil heat flux $G$ could then be negligibly small compared with the other heat fluxes. Here, the daily mean $K_{\theta}\downarrow$ calculated and the wind speed, $U_{10}$ ($U_z$ at $z$ = 10 m) at the Taiki Aerospace Research Field, and daily mean air temperature and relative humidity at site F are adopted to obtain the daily mean $T_{10}$ and $e_{10}$ values and the $T_{dew}$ values at $z$ = 10 m. Then, for daily mean air temperature, its spatial distribution or the elevation effect in the catchment should be taken into account. However, the daily mean air temperature at sites M, R1, F and P (**Figure 2.1**) did not indicate such a clear environmental lapse rate as -0.65°C/100 m, and the difference of daily air temperature was $|\Delta T| < 0.5\,°\mathrm{C}$ between site F and the other sites. This is probably due to the usual prevalence of sea wind from the Pacific Ocean (**Figure 2.1**). Finally, the $T_e$ value obtained by the successive approximation method yields:

$$Q_E = \lambda\cdot(\rho_a\,\varepsilon\,/p)\cdot\beta\,C_H\,U_{10}\{e_0(T_e) - e_{10}\} \qquad (3.14)$$

$$E = 8.64\times10^7\cdot\left(Q_E/\lambda\right)/\rho_w \qquad (3.15)$$

where $\rho_w$ is water density (kg m$^{-3}$) at $T_e$, and $E$ is evapotranspiration (mm day$^{-1}$).

Rainfall in the catchment did not have such a trend as an increase in rainfall with increasing altitude and, at less than 100 mm d$^{-1}$, was very similar in magnitude (**Hossain et al., 2015**). The

heavy rainfall in early May 2012 varied from 150 to 210 mm $d^{-1}$ in the catchment, but with no trend in altitude. Thus, rainfall data at site P (142 m asl in altitude) were employed as representative rainfall for modelling (**Figure 2.1**).

### 3.4 Model Performance Evaluation

The accuracy of model simulation results was determined by examining the **Nash and Sutcliffe (1970)** efficiency (*NSE*) and root mean square error (*RMSE*). The NSE simulation coefficient indicates how well the plot of observed values versus simulated values fits the 1:1 line. If the NSE value is less than zero, the model prediction is unacceptable or poor. If the value is one, then the model prediction is perfect (**Santhi et al., 2001**). Essentially, when the *NSE* is close to one, the models are considered more accurate.

NSE is statistically defined as

$$NSE = 1 - \frac{\sum_i^n (X_{oi} - X_{si})^2}{\sum_i^n (X_{oi} - \overline{X}_{oi})^2} \qquad (3.16)$$

where $X_{oi}$ is the observed data on day i, $X_{si}$ is the simulated output on day i, $\overline{X}_{oi}$ is the average measured value during the study period, $\overline{X}_{si}$ is the average simulated value during the study period and n is the total number of the observed data.

The *RMSE* is a frequently used measure of the difference between values predicted by a model and the values actually observed from the environment that is being modelled. These individual differences are also called residuals, and the RMSE serves to aggregate them into a single measure of predictive power.

The *RMSE* of a model prediction with respect to the estimated variable $X_{si}$ is defined as the square root of the mean squared error

$$RMSE = \sqrt{\frac{\sum_i^n (X_{oi} - X_{si})^2}{n}} \qquad (3.17)$$

where $X_{oi}$ is observed values and $X_{si}$ is modelled values at time/place *i*. The calculated RMSE values will have units. The *RMSE* values can be used to distinguish model performance in a calibration period with that of a validation period as well as to compare the individual model performance to that of other predictive models.

### 3.5 Modelling discharge

In order to simulate daily mean discharge time series, the lumped tank model (**Sugawara, 1972**) was applied. Irrespective of a kind of conceptual model, the tank model may reflect the processes of percolation and resultant groundwater storage to produce both river discharge and groundwater leakage. The data sets for modelling are daily mean river discharge sediment load at site R1, daily precipitation at site P and daily evapotranspiration by the one-layer model in the rainfall seasons in 2011-2014. The tanks' layout for modelling is shown in **Figure 3.1**. Of the three sequential tanks, the lowest tank has an outlet at bottom for groundwater leakage. The side drainage from the top tank, the middle tank and the lowest tank corresponds to "surface flow", "intermediate flow" and "baseflow" to a river channel, respectively. The bottom drainage from the top tank and middle tank indicates the percolation of rainwater. The water input and output from the top tank correspond to rainfall and evapotranspiration, respectively. Actual evapotranspiration from the one-layer model is given as output from the top tank.

The 12 parameters for drainage ($a_{11}$, $a_{12}$, $b_1$, $a_2$, $b_2$, $a_3$, and $b_3$ in day$^{-1}$), initial storage ($h_1$, $h_2$, and $h_3$ in mm) and outlet heights ($h_{11}$ and $h_{12}$ in mm) in the tanks were numerically determined to give the best fit to the observed discharge in 2011-2014. The "best fit" means that, when the side drainage from the tanks is calculated in order of the top tank to the lowest tank and

compared with observed runoff rate, the Nash-Sutcliffe efficiency coefficient(*NSE*) takes a maximum of more than 0.8. The root-mean-square error, *RMSE* ($m^3s^{-1}$), was also calculated. Normally, to specify the 12 parameters' values, the "calibration" for simulation should be done for a certain period, and then, using the same values, the "validation" is performed for the other periods. Here I have chosen the year 2012 as a calibration period and 2011, 2013 and 2014 as a validation year. However, permeable bedrock and many faults in the catchment (**Figure 2.2**) seem to drastically change groundwater storage and groundwater leakage to the neighboring catchment year by year. Hence, the parameters to give the best fit were numerically obtained in 2012; using the calibrated parameters in 2012 we validated our calibrated model in other years 2011. 2013 and 2014 respectively and thereby, a difference of discharge into the river channel, groundwater storage change and groundwater leakage was discussed. Each of the side and bottom drainages from each tank is given as a storage function model by following equations:

$$q_{ij} = \begin{cases} a_{ij}(h_i(n) - h_{ij}) \cdot \left[1 - \exp\left\{-(\sum_j a_{ij} + b_i)\right\}\right] / (\sum_j a_{ij} + b_i) & \text{when } h_i > h_{ij} \quad (i = 1, j = 1, 2) \\ 0 & \text{when } h_i \le h_{ij} \quad (i = 1,\ j = 1, 2) \end{cases} \tag{3.18}$$

$$q_i = a_i(h_i(n) - h_i) \cdot \left[1 - \exp\left\{-(a_i + b_i)\right\}\right] / (a_i + b_i) \qquad (i = 2,3) \tag{3.19}$$

$$p_i = b_i \cdot h_i(n) \cdot \left[1 - \exp\left\{-(\sum_j a_{ij} + b_i)\right\}\right] / (\sum_j a_{ij} + b_i) \qquad (i = 1, j = 1, 2) \tag{3.20}$$

$$p_i = b_i \cdot h_i(n) \cdot \left[1 - \exp\left\{-(a_i + b_i)\right\}\right] / (a_i + b_i) \qquad (i = 2, 3) \tag{3.21}$$

$$h_i(n+1) = \begin{cases} h_i(n) - \Delta t \cdot \sum_j q_{ij}(n) - p_i(n) \cdot \Delta t + P(n) \cdot \Delta t - E(n) \cdot \Delta t & (i = 1,\ j = 1,2) \\ \\ h_i(n) - q_i(n) \cdot \Delta t - p_i(n) \cdot \Delta t + p_{i-1}(n) \cdot \Delta t & (i = 2, 3) \end{cases} \quad (3.22)$$

where $q_{ij}$ ($i$ =1, $j$=1, 2) is side drainage (mm day$^{-1}$) from the top tank, $q_i$ ($i$ = 2, 3) is side drainage from the middle and lowest tanks, $p_i$ ($i$ =1, 2, 3) is bottom drainage (mm day$^{-1}$) from each tank, $P$ is rainfall (mm day$^{-1}$), $\Delta t$ is a time step (here, a day) and $n$ is the day number. The $p_3$ in Equation (3.21) corresponds to groundwater leakage into the neighboring catchment and others. The ($q_{11}$ + $q_{12}$) from Equation (3.18) expresses surface flow produced in the surface soil layer of forest or grassland, while $q_2$ and $q_3$ depict intermediate flow and baseflow in the intermediate to lower soil layer and in the lower soil layer to bedrock, respectively. The sum, i.e., $q_r$ = ($q_{11}$ + $q_{12}$ + $q_2$ + $q_3$), produces river flow as daily runoff rate (mm day$^{-1}$), which is converted into river discharge $Q_{cal}$ (m$^3$ s$^{-1}$) by $Q_{cal}$ = 0.001·$A$·$q_r$/86400 (catchment area, $A$=6.247×10$^7$ m$^2$) for comparison with observed discharge.

### 3.6 Modelling sediment load

Referring to some previous researches of identifying sediment sources (**Walling, 1974**; **Morgan, 1995**; **Asselman, 2000**; **Kido et al., 2007**; **Wada et al., 2011**), suspended sediment load, $L_{cal}$ (kg s$^{-1}$), was calculated as power function of simulated river discharge and drainage as follows:

$$L_{cal} = aQ_{surf}{}^{b} + cQ_{cal}{}^{d} \quad (3.23)$$

where $Q_{surf}$ is surface flow ($m^3$ $s^{-1}$), calculated by $Q_{surf} = 0.001 \cdot A \cdot (q_{11}+q_{12})/86400$, $Q_{cal}$ is simulated river discharge, and *a*, *b*, *c* and *d* are empirical coefficients. In the right side of Equation (3.23), the first term indicates that soil erosion and transport occurs on the catchment slope by surface flow or overland flow, and the second term means that a river channel provides a sediment source such that the fluvial resuspension of sediment deposited previously in the channel occurs. It is assumed that the intermediate flow and base flow neither erode nor transport any sediment. The parameters, *a*, *b*, *c* and *d*, were numerically decided to give the best fit to observed sediment load time series at $NSE > 0.8$ as that for the simulation of discharge time series. Considering the order of sediment erosion and transport in a catchment, first, the first term in Equation (3.23) was calculated until getting a maximum *NSE*, and then the second term was calculated until obtaining a higher maximum *NSE*.

### 3.7 Calculated results

**Figure 3.2** shows calculated evapotranspiration and observed rainfall from April to November in the years 2011, 2012, 2013 and 2014. Here I have calculated the evapotranspiration by one layer model. The total rainfall in the years 2011, 2012, 2013 and 2014 were 979.00 mm, 1115.5 mm, 1177.0 mm and 914.5 mm respectively whereas evapotranspiration were 365.4 mm, 343.1 mm, 356.9 mm and 419.2 mm respectively. Evapotranspiration values with variability of ca. 61 %, depending on catchment slope angle and slope aspect (**Hossain et al., 2015**). Here we have observed that highest evapotranspiration (419.2 mm) in these four years was occurred in the year 2014 where rainfall amount (914.5 mm) was lowest and the lowest evapotranspiration (343.1 mm) was occurred in 2012 where amount of rainfall was highest (1177.0 mm).

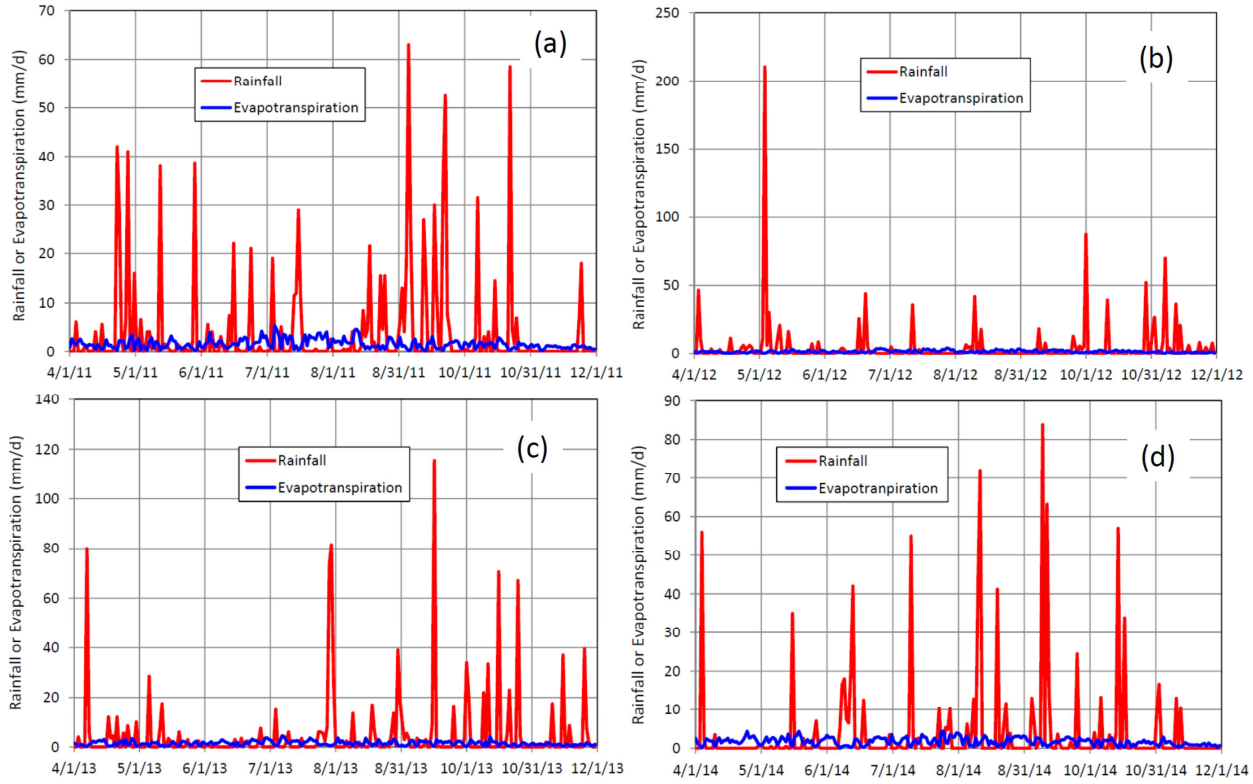


**Fig. 3.2** Calculated evapotranspiration and observed rainfall in (a) 2011, (b) 2012, (c) 2013 and (d) 2014

.

Calculated and observed discharge in April – November of 2011-2014 is shown in **Figure 3.3**. I calibrated the model in 2012 (**Fig. 3.3(a)**) and validated in 2011, 2013 and 2013. The simulation of discharge is very reasonable with *NSE*=0.891 in calibration period 2012 and 0.740, 0.780 and 0.804 in validation period in 2011, 2013 and 2014 respectively. *RMSE* were then1.25 $m^3$ $s^{-1}$, 0.883 $m^3$ $s^{-1}$, 1.51 $m^3$ $s^{-1}$ and 1.19 $m^3$ $s^{-1}$ in 2012, 2011, 2013 and 2014 respectively. The calibrated parameters' values in 2012 to give the best fit are shown in **Table 3**. The initial soil storage relatively very large in the lowest tank in 2013 and in 2012 ($h_3$=150 mm and 53 mm). The flow components separated in the tank model are shown in **Figure 3.4**. As expected, the surface flow is sensitive to rainfall and constitutes the major part in river runoff events. Probably reflecting faults and permeable bedrocks in the catchment, the baseflow or groundwater leakage

occupies the large portion of water flow on or below the catchment slope, especially in 2013, and

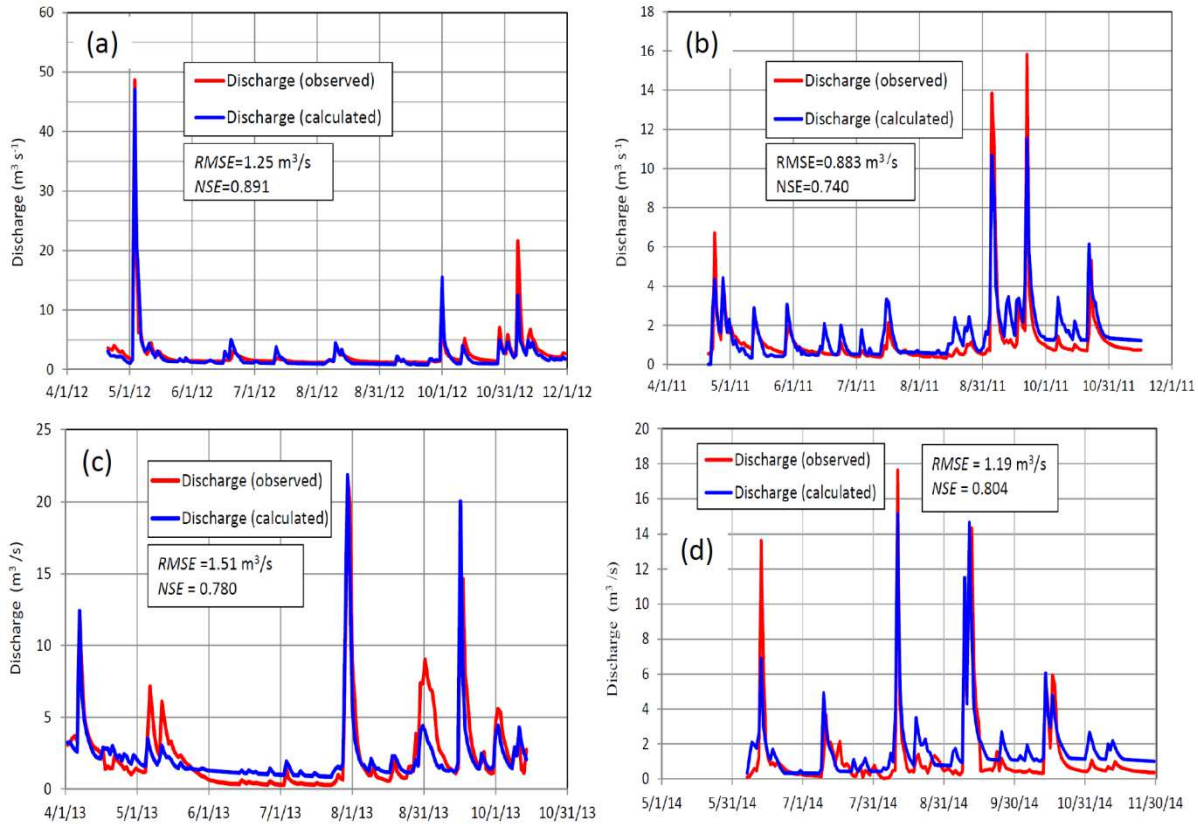


**Fig. 3.3** Discharge simulation at site R1 (a) Calibration 2012 (b) validation 2011(c) validation 2013 (d) validation 2014.

2011. Total daily runoff rates of flow components over the period of 1 April – 16 November 2011, 1 April -30 November 2012, 2 April – 14 October 2013 and 6 June – 30 November 2014 are 232.33 mm, 353.33 mm, 247.00 mm, 227.00 for surface flow, 210.00 mm. The intermediate flow in the years 2011, 2012, 2013 and 20114 were 58. 5%, 36.4%, 38.5% and 39.0% respectively. In these four years surface flow (51.5 %) followed by intermediate flow (48.5%) is dominating in the year 2011. Surface flow and intermediate are occupied the significant part of the total flow in all the four years because of high permeability of sandy tephra (Tarumae **Ta-b** )

layer of late Pleistocene at the depth of 30-40 cm in the forest soil layer (**Table 1**).

**Table 3** Parameters in the tank model and power function, giving the best fit to observed discharge and sediment load of 2011 - 2014

| Calibrated Parameters 2012 | $a_{11}$ ($s^{-1}$) | $a_{12}$ ($s^{-1}$) | $h_{11}$ (mm) | $h_{12}$ (mm) | $b_1$ ($s^{-1}$) | $a_2$ ($s^{-1}$) | $b_2$ ($s^{-1}$) | $a_3$ ($s^{-1}$) | $b_3$ ($s^{-1}$) |
|---|---|---|---|---|---|---|---|---|---|
| | 0.300 | 0.130 | 52.000 | 0.000 | 0.310 | 0.006 | 0.002 | 0.016 | 0.03 |

| Initial Soil moisture | $h_1$ (mm) | $h_2$ (mm) | $h_3$ (mm) |
|---|---|---|---|
| 2011 | 11.0 | 0.0 | 0.0 |
| 2012 | 79.0 | 155.0 | 53.0 |
| 2013 | 23.0 | 268.0 | 150.0 |
| 2014 | 0.0 | 0.0 | 0.0 |

| Sediment Parameters | *a* | *b* | *c* | *d* |
|---|---|---|---|---|
| 2011 | 0.160 | 2.010 | 0.023 | 1.16 |
| 2012 | 0.110 | 1.520 | 0.121 | 1.21 |
| 2013 | 0.900 | 0.930 | 0.050 | 1.29 |
| 2014 | 0.105 | 1.580 | 0.082 | 1.11 |

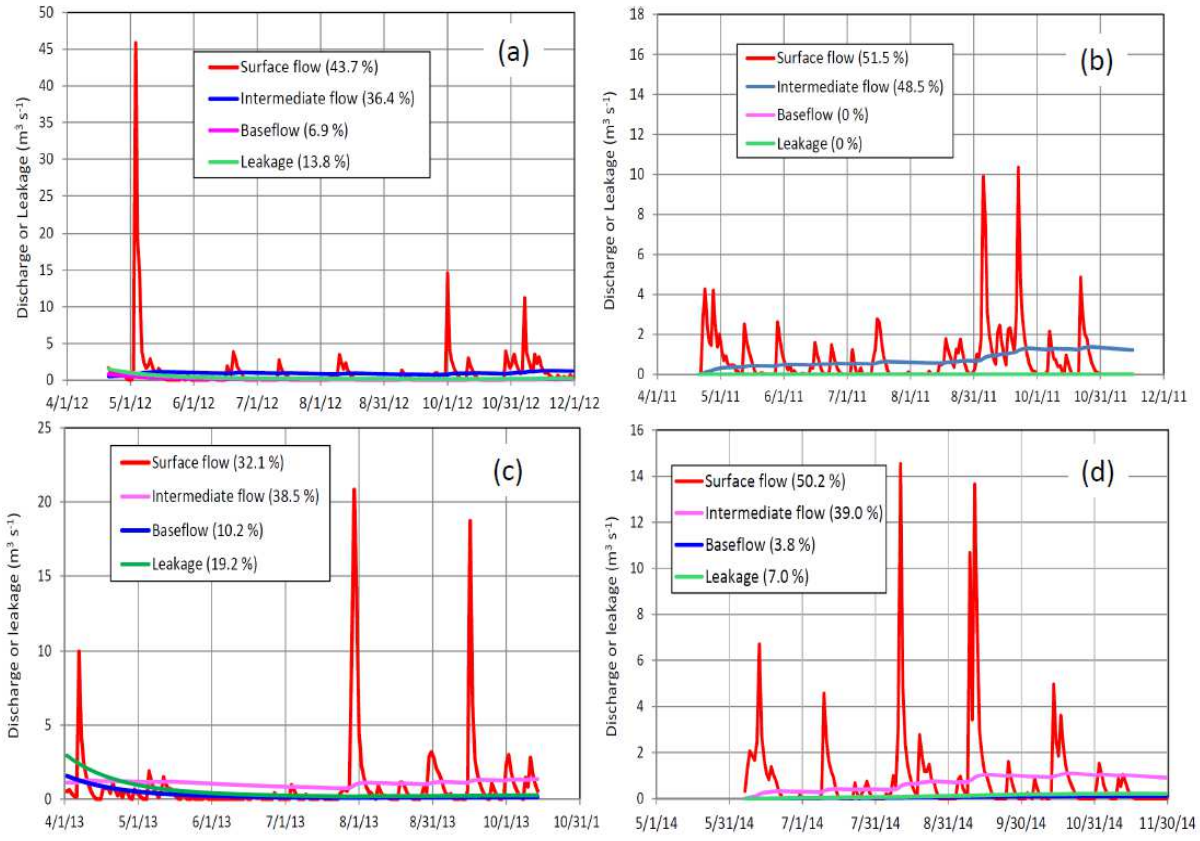


**Fig. 3.4** Time series and occupation rate of flow components separated by the tank model for (a) 2012 and (b) 2011, (c) 2013, (d) 2014.

**Figure 3.5** shows simulated results of sediment load in (a) 2011, (b) 2012, (c) 2013 and (d) 2014. The simulation is reasonable, showing high *NSE* values at 0.929, 0.917, 0.867 and 0.737 in

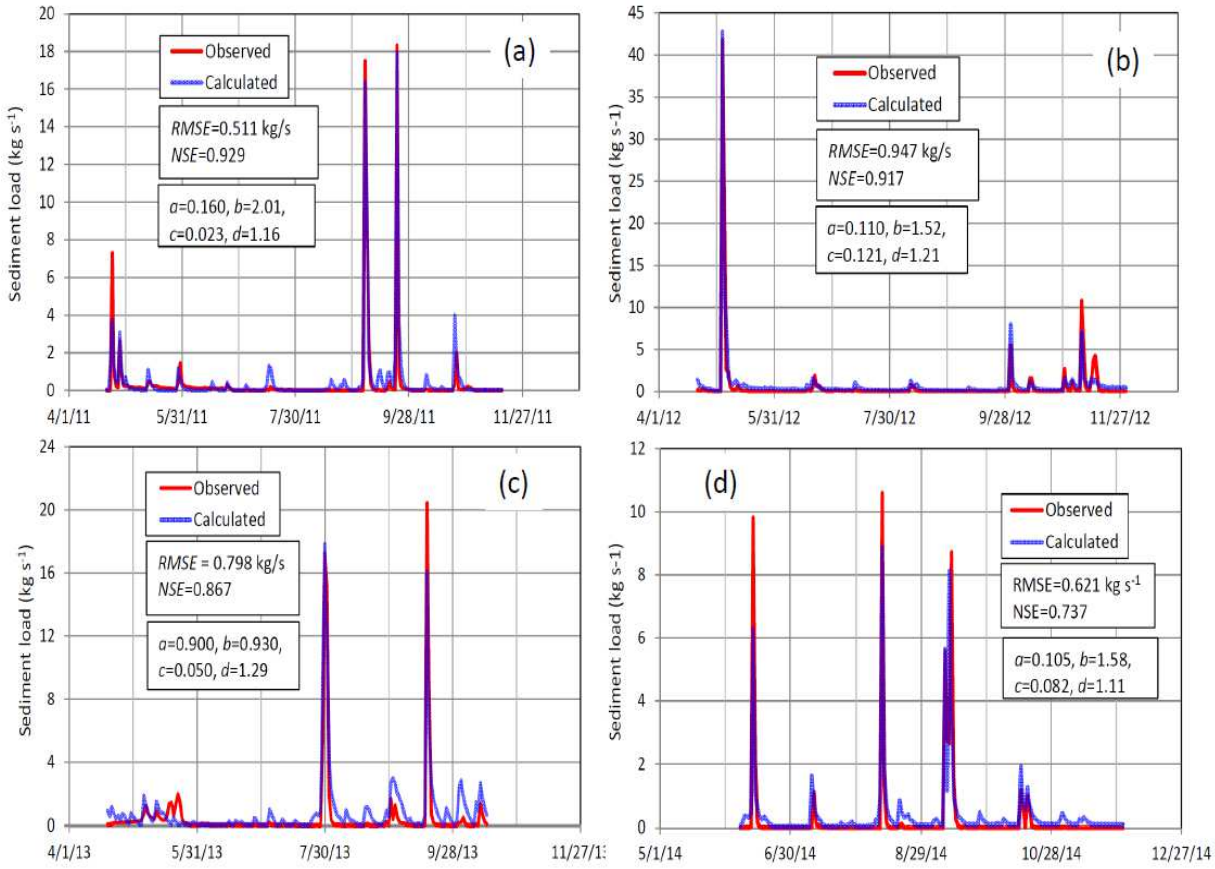


**Fig. 3.5** Simulated results of sediment load by the coupling with power function (a) 2011, (b) 2012, (c) 2013 and (d) 2014.

years 2011, 2012, 2013 and 2014 respectively. The *RMSE* values were then 0.511 kg $s^{-1}$ in 2011, 0.917 kg $s^{-1}$ in 2012, 0.798 kg $s^{-1}$ in 2013 and 0.621 kg $s^{-1}$ in 2014 respectively. Contribution rate of surface flow and river flow for sediment erosion and transport is comparable at 91.3 % and 8.7 % in 2011, at 49.4 % and 50.6 % in 2012, 82.1 % and 17.9 % in 2013 and 60.4 % and 39.6 % in 2014 respectively. However, sediment erosion and transport by surface flow occurs only in runoff events, while that by river flow appears at all times, including non-rainfall periods. These agents seem to be very reasonable, but to know how the "surface flow" in reality occurs on the

catchment slope is important. The *b* and *d* values in Equation (3.21) are very similar in the period of 2011- 2014 (**Table 3**). The *b* and *d* coefficients probably indicate the sediment erodibility such as grain size and mineralogy, thus being peculiar to the catchment, and the *a* and *b* coefficients the sediment availability for erosion, being changeable year by year (**Wada et al. , 2011)**.

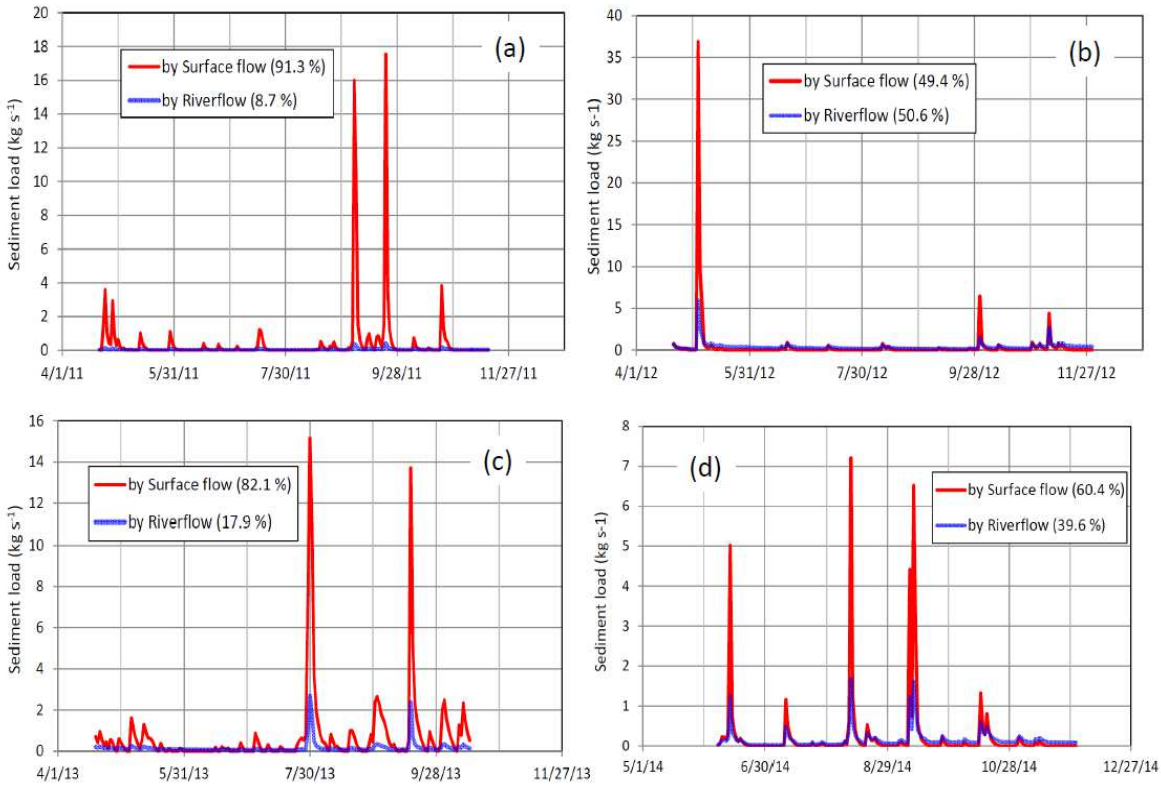


**Fig. 3.6** Contribution of sediment transport by surface flow and river by the tank model for (a) 2011, (b) 2012, (c) 2013 and (d) 2014.

### 3.8 Sensitivity analysis

The evapotranspiration estimated by the one-layer model has the 80 % variability, because downward shortwave radiation $K_\theta\downarrow$ in Equation (3.1) is seriously affected by the angle and aspect of the catchment slope with mean of 34.66° and 176.6° (clockwise from north at 0°) and standard deviation of 24.20° and 79.0°, respectively (**Hossain et al., 2015**). In sensitivity analysis

for modelling, the variability of evapotranspiration should be considered. For the discharge simulation, variation of *NSE* values was explored by changing the 11 parameters' values excluding $h_2$ at 0 mm in 2011- 2012. As a result, two parameters, $h_{11}$ and $a_{11}$, were most sensitive to a decrease in *NSE* values; the *NSE* value decreased from 0.919 to 0.469 in 2011 and from 0.920 to 0.880 in 2012 by a change of $h_{11}$ values at ± 40 %, and from 0.919 to 0.864 in 2011 and from 0.920 to 0.883 in 2012 by a change of $a_{11}$ values at ± 40 %. Hence, again, to know how the "surface flow" in reality occurs on the catchment slope is important, in order to clarify processes of discharging to the river channel.

For the simulation of sediment load, the sensitivity analysis of the parameters, *a*, *b*, *c* and *d*, in Equation (3.21) was conducted. As a result, the parameter, *b*, was very sensitive to *NSE* values, which became negative for a change of *b* values at ± 20 %. The parameter, *a*, secondly decreased *NSE* values to 0.808 in 2011 and to 0.802 in 2012 for a change of *a* values at ± 40 %. The parameters, *c* and *d*, did not give a great decrease in *NSE* values, showing 0.946 in 2011 and 0.856 in 2012 at lowest for the ± 40 % change in *c* and *d* values. Hence, probably, the specification of grain size, mineralogy, etc. for the catchment slope soil to be eroded and transported is important.

# CHAPTER FOUR

## SWAT MODEL

### 4.1 SWAT Modelling

Soil and Water Assessment Tool (SWAT) is a physical process based model to simulate continuous-time landscape processes at a catchment scale. The sediment yield model used in this study is the SWAT model. It is a comprehensive process-based model that simulates discharge sediment and chemical fluxes in watersheds under varying climatic conditions, soil properties, stream channel characteristics, land use and agricultural management (**Jayakrishnan et al., 2005**; **Talebizadeh et al., 2010**). The SWAT model has been applied to enhance understanding of sediment loss and transport processes over a wide range of environments around the world (**Oeurng et al., 2011**). For sediment yield modelling, **Mukundan et al. (2010)** examined the suitability of SWAT at the North Fork Broad River catchment located in the Piedmont region of Georgia, and their results suggested that the SWAT model is a better substitute than the sediment rating curve for estimating sediment yield. Many researchers have reported that the SWAT model predicted reasonable results for sediment yield estimation (especially on monthly and yearly timescales) when accurate input data and model parameterization were provided (**Chu et al., 2004**; **Saghafian et al., 2012**).

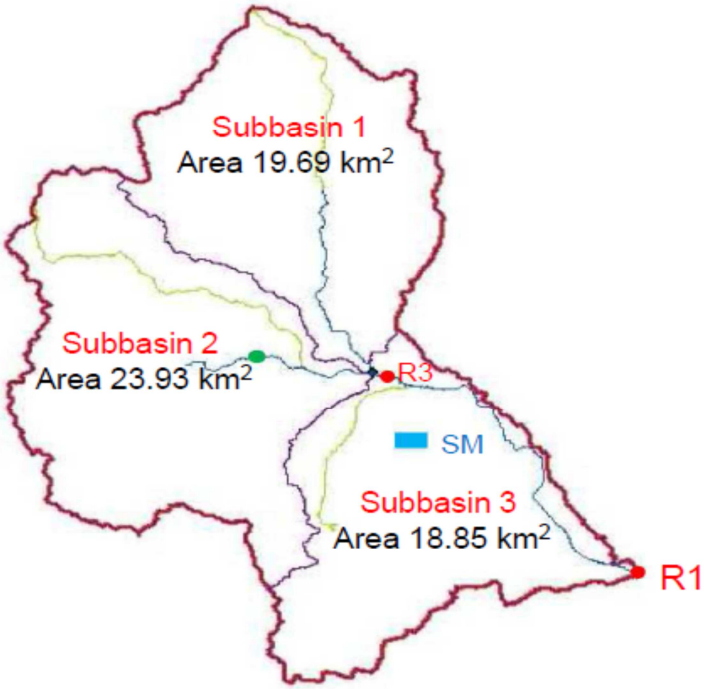


**Fig. 4.1** Oikamani River basin separated by three subbasions

Here, the drainage basin is divided into three sub-basins as sub-basin into hydrological response unit (HRU) based on soil type, land use and slope classes **(Fig. 4.1)**. The SWAT model predicts the hydrology at each HRU using the water balance equation, which includes daily rainfall, runoff, actual and potential evapotranspiration using the Penman–Monteith equation, percolation and return flow components. The model can estimate soil erosion from the landscape and in-stream depositional and erosive processes. The sediment yield from the landscape is calculated using the modified Universal Soil Loss Equation (MUSLE; **Williams, 1975**) and runoff energy is used to detach and transport sediment. Sediment deposition and erosion in the stream channel are both calculated during sediment routing. The maximum amount of sediment

that can be transported from a reach segment during the sediment routing in a river channel is determined by the modified Bagnold's (**Bagnold, 1977**).

## 4.2 MODEL INPUT

The inputs required by the SWAT model are daily weather data of precipitation, maximum and minimum temperature, wind speed, solar radiation and relative humidity, which were obtained from the weather stations' records at five weather stations at the Taiki Aerospace Research Field (rainfall, solar radiation, and wind speed and direction) 9.6 km south of site R1, Taiki town (snow depth) 18.9 km southwest of site R1, and site F, site P and site M in the Oikamanai River basin in 2011 – 2014 (**Fig. 2.1**). Digital elevation model (DEM) data (**Fig. 2.1**) was prepared using a digital map with a 30 m grid elevation created from a 1:25 000 topographic map published by the Japanese Geographical Survey Institute (GSI, http://nlftp.mlit.go.jp/ksj/jpgis/jpgis_datalist.html). GIS-referenced soil data (**Fig. 4.2**) were extracted from a 1:50 000 soil map of the Fundamental Land Classification Survey developed by the Hokkaido Regional Development Bureau (www.agri.hro.or.jp/chuo/kankyou/soilmap/html/map_index.htm). A land use map (1:25 000) based on land cover in 2005 was obtained from the GSI (**Fig. 4.2**).

## 4.3 Land Use and Soil Distribution

The Oikamani River basin is covered by five types of land (**Fig. 4.2**) among them most of the land is covered by forest (88.3%) and farmland (10.6%), farmland is mainly grass land area.

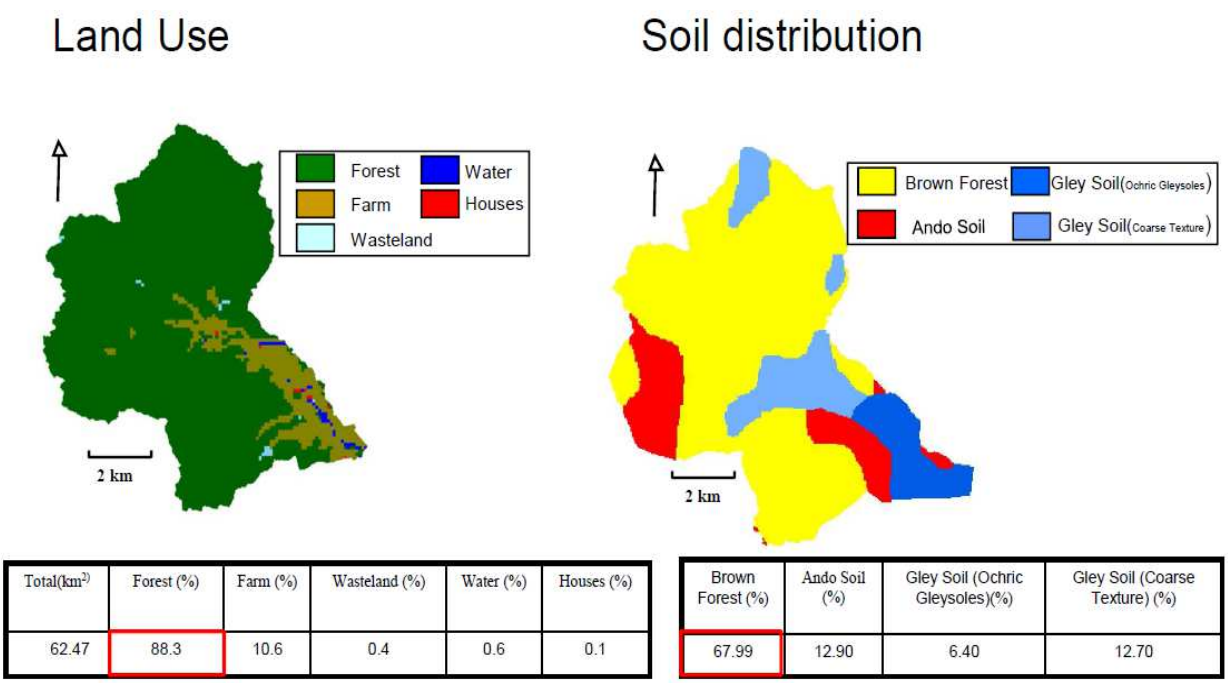


| Total(km²) | Forest (%) | Farm (%) | Wasteland (%) | Water (%) | Houses (%) |
|---|---|---|---|---|---|
| 62.47 | 88.3 | 10.6 | 0.4 | 0.6 | 0.1 |

| Brown Forest (%) | Ando Soil (%) | Gley Soil (Ochric Gleysoles)(%) | Gley Soil (Coarse Texture) (%) |
|---|---|---|---|
| 67.99 | 12.90 | 6.40 | 12.70 |

**Fig. 4.2** Land Use and Soil distribution

Four types of soil is distributed in these study area where main soil is brown forested soil (67.99 %) (**Fig. 4.2**) followed by ando and gley soil. From here we have seen that land use and soil are dominated by forest land cover and brown forest soil. So we can say that this study area is forested River catchment influenced by slope failure (**Fig. 2.2**).

### 4.4 Discharge Simulation by SWAT Model

The SWAT model is a spatially distributed, physically process-based model for predicting the movement of water, sediment and chemicals in complex catchments with varying soils, land uses and management conditions over long periods of time. Major model components include weather, hydrology, soil temperature and properties, plant growth, nutrients, pesticides, bacteria and pathogens, and land management. The SWAT model simulates water and nutrient cycles within numerous sub-basins, which are then further subdivided into hydrologic response units

that consist of homogeneous land use, soil and terrain characteristics. These steps resulted in 26 individual HRUs within the 3 sub-basins in the Oikamanai forested River watershed.

In a conservative environment, the total water entering channels every day from each HRU in the SWAT model can be derived from

$$Q_{flow} = \left(Q_{surf} + Q_{lat} + Q_{gw}\right) \times \mathrm{HRU}_{\mathrm{area}} \qquad (4.1)$$

where $Q_{flow}\,(\mathrm{mm}^3)$, is the total water entering the channel of the sub-basin where the HRU is located, $Q_{surf}$ is surface runoff yield (mm), $Q_{lat}$ is lateral flow yield (mm), $Q_{gw}$ is groundwater yield (mm) and $\mathrm{HRU}_{\mathrm{area}}$ is the HRU area ($\mathrm{mm}^2$). The surface runoff $Q_{surf}$ is defined as

$$Q_{surf} = \frac{(R_{day} - I_a)^2}{(R_{day} - I_a + S)} \qquad (4.2)$$

where $Q_{suf}$ is the accumulation runoff or rainfall excess $\left(\mathrm{mm\,H_2O}\right)$, $R_{day}$ is the rainfall depth for the day $\left(\mathrm{mm\,H_2O}\right)$, $I_a$ is the initial abstractions which includes surface storage, interception and infiltration prior to runoff $\left(\mathrm{mm\,H_2O}\right)$, and $S$ is the retention parameter $\left(\mathrm{mm\,H_2O}\right)$. The retention parameter varies spatially due to changes in soils, land use, management and slope and temporally due to changes in soil water content. The retention parameter is defined as:

$$S = 25.4\left(\frac{1000}{CN} - 10\right) \qquad (4.3)$$

where CN is the curve number for the day. The initial abstractions $I_a$ is commonly approximated as $0.2S$ and Equation (4.2) becomes

$$Q_{surf} = \frac{(R_{day} - 0.2\,S)^2}{(R_{day} + 0.8\,S)} \qquad (4.4)$$

Runoff will only occur when $R_{day} > I_a$.

### 4.5 Model Calibration and Validation

The SWAT model was first calibrated using SWAT Calibration and Uncertainty Programs (CUP) with the Sequential Uncertainty Fitting (SUFI2) calibration and uncertainty analysis routine (**Abbaspour, 2007**). Then the calibration of flow and sediment was performed manually to obtain a good match between the observed and simulated values. Key hydrological and sediment-related parameters were selected, based on global sensitivity analysis. Calibration is an effort to better parameterize a model to a given set of local conditions, thereby reducing the prediction uncertainty. Model calibration is performed by carefully selecting values for model input parameters by comparing model predictions for a given set of conditions with observed data for the same conditions. Model validation is the process of demonstrating that a given site-specific model is capable of making sufficiently accurate simulations. Validation involves running a model using parameters that were determined during the calibration process, and comparing the predictions to observed data not used in the calibration. Calibration and validation are typically performed by splitting the available observed data into two datasets: one for calibration, and another for validation. Data are most frequently split by time periods (**Arnold et al., 2012**). In this study, parameters calibrated for streamflow are shown in **Table 4**. Sensitive parameters are calibrated within their acceptable ranges to match the simulated streamflow with the observed streamflow (**Table 4**). In **Figure 2.4**, snow depth in 2012 is nearly two times of 2011; it indicates that initial condition of soil water content, groundwater storage, and soil parameters are different in different years. So here we have simulated discharge in year wise that is a single year of non-snowfall and non-snowmelt season are taken for calibration and another year is taken as validation period. Here period April to November of 2012 is considering for calibration and April to November of 2011, 2013 and 2014 for validation (**Fig. 4.3**). The

calibrated parameters in 2012 are showed in **Table 4**. Here the parameters are calibrated within their acceptable ranges to match the simulated streamflow. In the year 2012 the most sensitive parameter is runoff curve number (CN2.mgt) followed by effective hydraulic conductivity in main channel alluvium (mm/h) (CH_K2.rte), available water capacity of the soil layer (SOL_AWC.sol), and maximum canopy storage (CANMX.hru) etc. (**Table 4**).

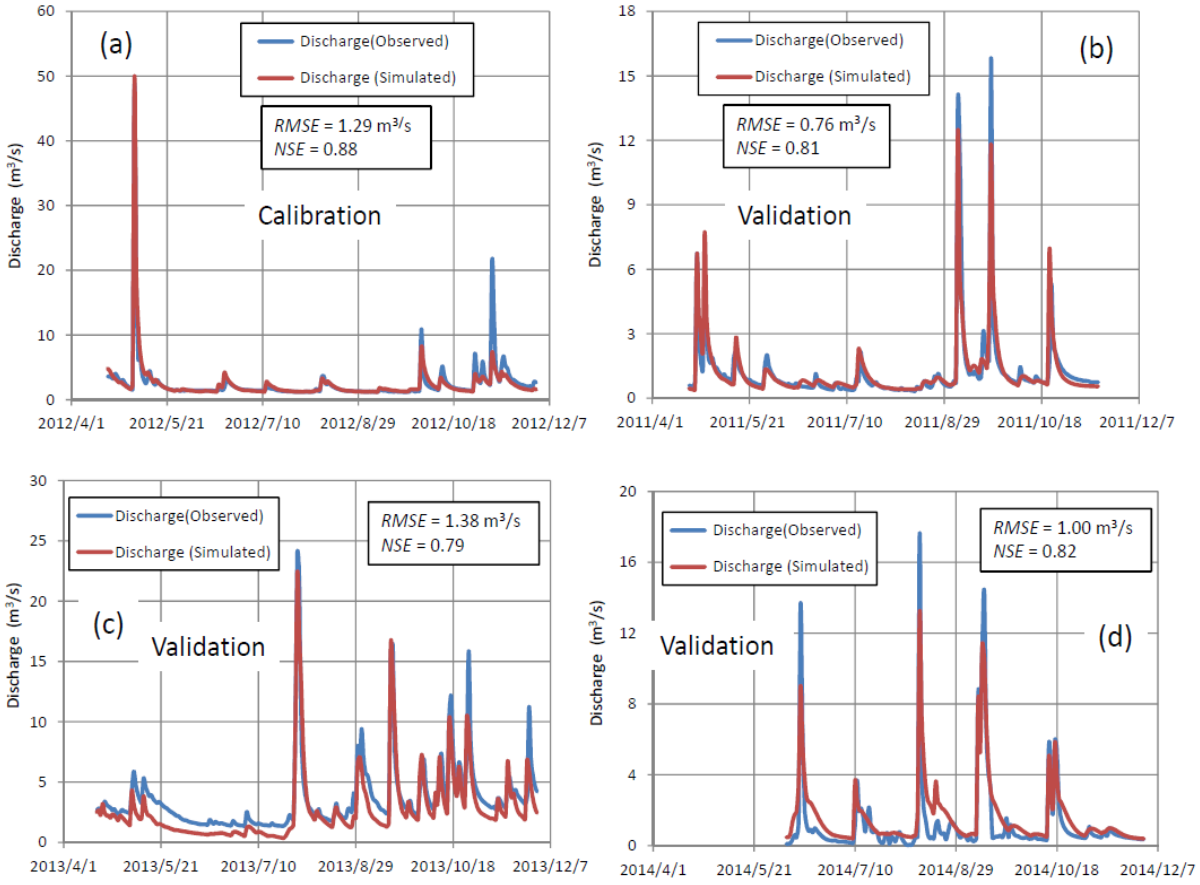


**Fig. 4.3** Discharge simulation at site R1 (a) calibration in 2012, (b) validation in 2011, (c) validation in 2013, (d) validation in 2014.

**Table 4** presents the calibrated parameters for discharge, whereas **Figure 4.3** graphically illustrates the comparison between the observed and simulated daily discharge at the main outlet R1 of the Oikamanai River watershed. The statistical performance of the SWAT for daily streamflow estimation was satisfactory NSE value in calibration year 2012 is 0.88 and in validation years the values are 0.81, 0.79 and 0.82 respectively in the year 2011, 2013 and 2014.

However the simulated peak discharge is overestimated in early May of calibration year in 2012 because of heavy rainfall event affected the model simulation. To reduced model discharge in this event in 2012 calibration process changed some parameters values which affected the validation period by underestimated peak discharged during some big rainfall periods **Fig. 4.3** (b), (c) and (d). In addition it might be because precipitation duration and intensity are not being considered by the soil conservation services (SCS) curve number (CN) method (**SCS, 1972**) for simulation of streamflow in SWAT model as reported by **Phomcha et al. (2011)**. This limitation might be more profound for the heavy rainfall events.

**Table 4** Parameters for streamflow calibration performed at site R1 of the Oikamanai River watershed in 2012

| No. | Parameters | Definition of Parameters | Fitted values |
|---|---|---|---|
| 1 | r_CN2.mgt | Initial SSC runoff curve number for moisture contidition II | 0.72 |
| 2 | v_CH_K2.rte | Effective hydraulic conductivity in main channel alluvium (mm/h) | 17.62 |
| 3 | r_SOL_AWC.sol | Available water capacity of the soil layer | -0.94 |
| 4 | v_CANMX.hru | Maximum canopy storage | 4.49 |
| 5 | v_GWQMN.gw | Treshold depth of water in the shallow aquifer required for return flow to occur (mm) | 830.11 |
| 6 | v_REVAPMN.gw | Threshold depth of water in the shallow aquifer for "revap" to occur (mm) | 521.53 |
| 7 | v_ESCO.hru | Soil evaporation compensation factor | 0.99 |
| 8 | v_SURLAG.bsn | Surface runoff lag time | 11.94 |
| 9 | v_ALPHA_BF.gw | Baseflow alpha factor (days) | 0.99 |
| 10 | v_GW_REVAP.gw | Groundwater "revap" coefficient. | 0.08 |
| 11 | v_EPCO.hru | Plant uptake compensation factor | 0.01 |
| 12 | v_RCHRG_DP.gw | Deep aquifer percolation fraction | 0.86 |

The extension (e.g., .mgt) refers to the SWAT input file where the parameter occurs.
The qualifier (v_) refers to the substitution of a parameter by a value from the given range.
The qualifier (r_ ) refers to relative change in the parameter where the value from the SWAT database is multiplied by 1 plus a factor in the given range.

## 4.6 Sediment load simulation

Transport of sediment, nutrients and pesticides from land areas to water bodies is a consequence of weathering that acts on landforms. Soil and water conservation planning requires knowledge of the relations between factors that cause loss of soil and water and those that help to reduce such losses. Erosion is the wearing down of a landscape over time. It includes the detachment, transport, and deposition of soil particles by the erosion forces of raindrop and flow of water.

A land area contains rills and channels. Raindrop impact can detach soil particles on unprotected land surfaces between rills and initiate transport of these particles to the rills. From the small rills, the particles moves to larger rills, then into ephemeral channels and then into continuously flowing rivers. Entrainment and deposition of particles can occur at any point along the path. When erosion occurs without human influences, it is called geologic erosion. Accelerated erosion occurs when human activity increases the rate of erosion.

Erosion is a matter of concern to watershed and natural resource managers. Two of the main reasons reservoirs are built are water supply and flood control. Erosion upstream of a reservoir deposits sediment in the bottom of the reservoir which lowers the reservoir's water-holding capacity and consequently its usefulness for both of these purposes. The soil surface is the part of the soil profile highest in organic matter and nutrients. Organic matter forms complexes with soil particles so that erosion of the soil particles will also remove nutrients. Excessive erosion can deplete soil reserves of nitrogen and phosphorous needed by plants to grow and extreme erosion can degrade the soil to the point that it is unable to support plant life. If erosion is severe and widespread enough, the water balance of a watershed can be altered-remember that most water is lost from a watershed via evapotranspiration. Erosion caused by rainfall and runoff is compared with the Modified Universal Soil Lose Equation (MUSLE) (**Williams, 1975**). MUSLE is a modified version of the Universal Soil Lose Equation (USLE) developed by Wischmeier and Smith (1965, 1978).

USLE predicts average annual gross erosion as a function of rainfall energy. In MUSLE, the rainfall energy factor is replaced with a runoff factor. This improves the sediment yield prediction, eliminates the need for delivery ratios, and allows the equation to be applied to individual storm events. Sediment yield prediction is improved because runoff is a function of

antecedent moisture condition as well as rainfall energy. Delivery ratios (the sediment yield at any point along the channel divided by the source erosion above that point) are required by USLE because the rainfall factor represents energy used in detachment only. Delivery ratios are not needed with MUSLE because the runoff factor represents energy used in detaching and transporting sediment. The modified universal soil loss equation (MUSLE) (**Williams, 1995**) to compute soil erosion on the catchment slope is

$$Sed = 11.8(Q_{surf} \cdot q_{peak} \cdot area_{hru})^{0.56} \cdot K_{USLE} \cdot C_{USLE} \cdot P_{USLE} \cdot LS_{USLE} \cdot CFRG \qquad (4.5)$$

where *Sed* is the sediment load on a given day(metric tons), $Q_{surf}$ is the surface runoff volume $(\text{mm H}_2\text{O/ha})$, $q_{peak}$ is the peak runoff rate $(m^3/s)$, $area_{hru}$ is the area of the HRU(ha), $K_{USLE}$ is the USLE soil erodibility factor $(0.013\,\text{metric ton m}^2\,\text{hr}/(\text{m}^3 - \text{metric ton cm}))$, $C_{USLE}$ is the USLE cover and management factor, $P_{USLE}$ is the USLE support practice factor, $LS_{USLE}$ is the USLE topographic factor and *CFRG* is the coarse fragment factor.

Sediment transport in the river channel network is a function of two processes, deposition and degradation, operating simultaneously in the reach. From landscape component, SWAT keep tracks of the particle size distribution of eroded sediments and routes them though ponds, channels and surfaces water bodies. In the channel, degradation or deposition of sediment can occur depending on the stream power, the exposure of channel sides and bottom to the erosive force of the stream and the composition of the channel bank and bed sediment.

**Bagnold (1977)** defines the stream power definition as degradation is a function of channel slope and velocity. In SWAT 2012 version used simplified Bagnold's equation in such a way that the maximum amount of sediment that can be transported from a reach segment is a function of the peak channel velocity. The peak channel velocity $v_{ch.pk}$ is calculated:

$$v_{ch,pk} = \frac{q_{ch,pk}}{A_{ch}} \qquad (4.6)$$

where $q_{ch,pk}$ is the peak flow rate ($m^3/s$) and $A_{ch}$ is the cross sectional area of flow ($m^3/s$). the peak flow rate is defined as

$$q_{ch,pk} = prf \cdot q_{ch} \qquad (4.7)$$

where *prf* is the peak rate adjustment factor, and $q_{ch}$ is the average rate of flow ($m^3/s$). the maximum amount of sediment that can be transported from a reach segment is calculated:

$$conc_{sed,ch,mx} = c_{sp} \cdot v_{ch,pk}^{\ spexp} \qquad (4.8)$$

where $conc_{sed,ch,mx}$ is the maximum concentration of sediment that can be transported by water (ton/$m^3$ or kg/L), $c_{sp}$ is a coefficient defined by user, $v_{ch,pk}$ is the peak channel velocity (m/s), and *spexp* is an exponent defined by the user.

The maximum concentration of sediment calculated with (4.8) is compared to the concentration of sediment in the reach at the beginning of the time step, $conc_{sed,ch,i}$. If $conc_{sed,ch,i} > conc_{sed,ch,mx}$, deposition is the dominant process in the reach segment and the net amount of sediment deposition is calculated:

$$sed_{dep} = (conc_{sed,ch,i} - conc_{sed,ch,mx}) \cdot V_{ch} \qquad (4.9)$$

where $sed_{dep}$ is the amount of sediment deposited in the reach segment (metric tons), $V_{ch}$ is the volume in the reach segment ($m^3$ $H_2O$). If $conc_{sed,ch,i} < conc_{sed,ch,mx}$, degradation is the dominant process in the reach segment and the net amount of sediment reentrained is calculated:

$$sed_{\deg} = (conc_{sed,ch,mx} - conc_{sed,ch,i}) \cdot V_{ch} \cdot K_{CH} \cdot C_{CH} \qquad (4.10)$$

where $sed_{dep}$ is the amount of sediment reentrained in the reach segment (metric tons), $K_{CH}$, channel erodibility factor, $C_{CH}$ is channel cover factor.

The SWAT model is further used for sediment yield calibration following completion of discharge calibration process in the years 2011, 2012, 2013 and 2014. Sediment load simulation is a little bit difficult. Sediment can come from basin slope, slope failure (bank collapse and land slide), river bank erosion and river bed erosion respectively. Here I have simulated the sediment load simulation in the years 2011, 2012, 2013 and 2014 respectively (**Fig. 4.4)**.

**Table 5** presents the calibrated parameters for sediment simulation in the years 2011, 2012, 2013 and 2014 respectively. **Figure 4.4** generally indicates that the simulated daily sediment loads of the SWAT model and the observed values are comparable, yielding NSE of 0.74, 0.91, 0.75 and 0.76 in the years 2011, 2012, 2013 and 2014 respectively.

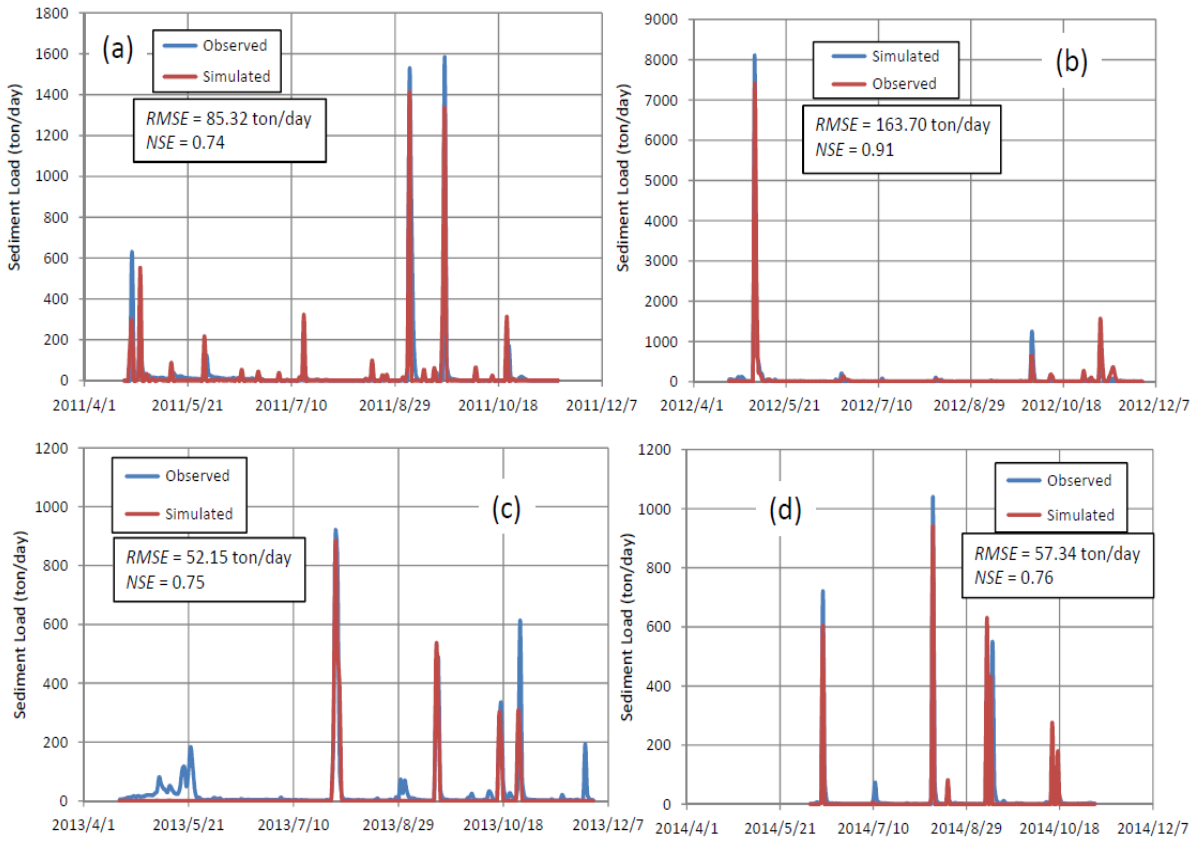


**Fig. 4.4** Sediment load simulation at site R1 in 2011(a), 2012 (b), 2013 (c) & 2014 (d

However, a comparison of the results indicates that the SWAT model might overestimate the sediment load for some high-flow events (**Fig. 4 (b)**) because in this time period rainfall was high moreover the SWAT model allows all the soil eroded by runoff to reach the river directly, without considering sediment deposition remaining on surface catchment areas. The results also indicate that the SWAT model underestimated the sediment load of some peak events (**Fig. 4(a), (c), (d)**). This might be because landslide and bank collapse is not considered and the sediment routing algorithm used in SWAT is very simplified. The topographic factor ($LS_{USLE}$) automatically estimated from the DEM in the SWAT model was found to contain errors (**Kim et al., 2009; Babel et al., 2011**), it partially explains the model inaccuracies for sediment yield estimation. With better accuracy and resolution of DEM and more reliable methods for derivation of the topographical variables related to LSUSLE, such as slope

**Table 5** Optimum values of sediment parameters in SWAT

| No. | Parameters | Definitiobn of Parameters | 2011 | 2012 | 2013 | 2014 |
|---|---|---|---|---|---|---|
| 1 | USLE_C(FRST).crop.dat | Forest land cover and management factor | 0.27 | 0.01 | 0.22 | 0.01 |
| 2 | USLE_C(PAST).crop.dat | Framland cover and management factor | 0.17 | 0.73 | 0.24 | 0.14 |
| 3 | USLE_P.mgt | USLE support practice factor | 0.04 | 0.42 | 0.17 | 0.88 |
| 4 | SPCON.bsn | Linear sediment reentrained parameter for channel routing | 0.01 | 0.01 | 0.01 | 0.00 |
| 5 | SPEXP.bsn | Exponent sediment reentrained parameter for channel routing | 1.38 | 1.29 | 1.34 | 0.97 |
| 6 | ADJ_PKR.bsn | Peak rate adjustment factor in the tributary channel | 1.59 | 1.16 | 0.79 | 0.53 |
| 7 | PRF.bsn | Peak rate adjustment factor in the main channel | 1.73 | 1.91 | 1.05 | 0.96 |
| 8 | CH_COV1.rte | Channel erodibility factor | 0.17 | 0.17 | 0.29 | 0.32 |
| 9 | CH_COV2.rte | Channel cover factor | 0.66 | 0.86 | 0.72 | 0.83 |
| 10 | USLE_K.sol | Soil erodibility factor | 0.03 | 0.02 | 0.33 | 0.12 |
| 11 | CH_BNK_BD.rte | Bulk density of channel bank sediment | 1.48 | 1.84 | 1.60 | 1.69 |
| 12 | CH_BED_BD.rte | Bulk density of channel bed sediment | 1.63 | 1.89 | 1.76 | 1.82 |

The most sensitive parameter for sediment load simulation are land cover and management factor (USLE _C (FRST), USLE _C (FRST)), USLE equation support practice factor (USLE_P.mgt), peak rate adjustment factor( PRF.bsn, ADJ_PKR.bsn) and soil erodibility factor (USLE_K.sol). Other parameters are nearly constant in the whole four years (**Table 5**).

# CHAPTER FIVE

## DISCHARGE AND SEDIMENT LOAD COMPARISON AT OUTLETS

### 5.1 Comparison of Discharge and Sediment load between at site R1 and site R3

We have two outlets of forested Oikamani River catchment at site R1 and at site R3 (**Fig.2.1**); main outlet at site R1 where we have observed discharge and sediment load data from April, 2011 and at site R3; meeting point of subbasin 1 and subbasin 2 we have observed data from July 2013. I monitored water level, turbidity, water and air pressure, water and air temperature at these two sites. So we will compare discharge, sediment load between site R1 and site R3 from July 2013 by observed data and SWAT model. **Figure 5.1** shows that observed daily discharge at site R1 always greater than that of site R3; it is normal since the site R3 is the upstream of the Oikamani River catchment whereas the site R1 is the main outlet of this catchment and all the discharge of this catchment passes though the main outlet R1. Here I did not consider the snowfall and snowmelt period and some data was missing from April 2014 to June 5, 2014, so discharge, sediment load and sediment yield graph is not continuous (**Fig.5.1, Fig. 5.2, Fig. 5.3**).

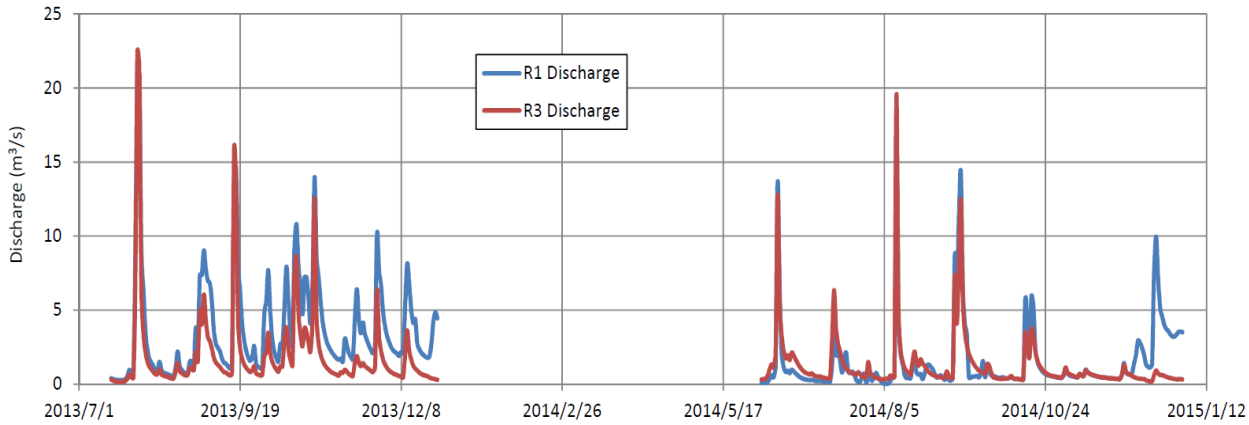


**Fig. 5.1** Daily observed discharge at sites R1 and R3

The sediment load at site R1 and R3 in **Figure 5.2** shows sediment load at site R3 always greater than that of site R1 whereas discharge at site R1 was larger than at site R3 (**Fig. 5.1**). The sediment load at site R3 more probably results from the relatively steep slope at upstream of site R3 and surface geology consists mostly of Neogene sedimentary rocks, which could frequently produce landslide by heavy rainfall or snowmelt (**Araiba et al. 2008**). Also the forest soils are accompanied by permeable tephra layers of Tarumae Ta-b and Shikotsu Spfa-1, easily producing surface failure.

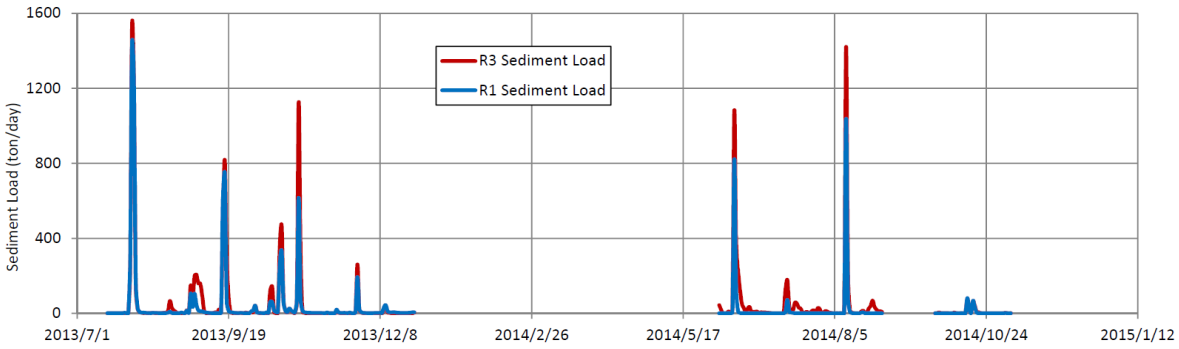


**Fig. 5.2** Sediment load observed at site R1 and site R3

**Figure 5.3** shows sediment yield at site R3 always greater than that of site R1; it indicates that transportation of sediment at site R1 is less than at site R3. Observed sediment yield in subbasin 3 is shown in **Figure 5.4**, here it is seen that most of the time sediment yield in subbasin 3 is negative, its mean that sediment input in subbasin 3 from site R3 is more compare to sediment output from site R1; it indicates that sediment deposition occur between site R3 and site R1. The upstream of site R3 is forested mountainous region with steep slope. The Neogene sedimentary rock accompanied with active faults frequently producing landslide and bank collapse under rainfall. The upstream of site R1 with gentle slope are composed of flood plain deposit of Holocene. This lower region is covered by farmland; mainly grass land, so probability

of soil erosion is very low. That's why most of the sediment originates in the upstream of site R3 of this catchment and deposits between site R1 and site R3.

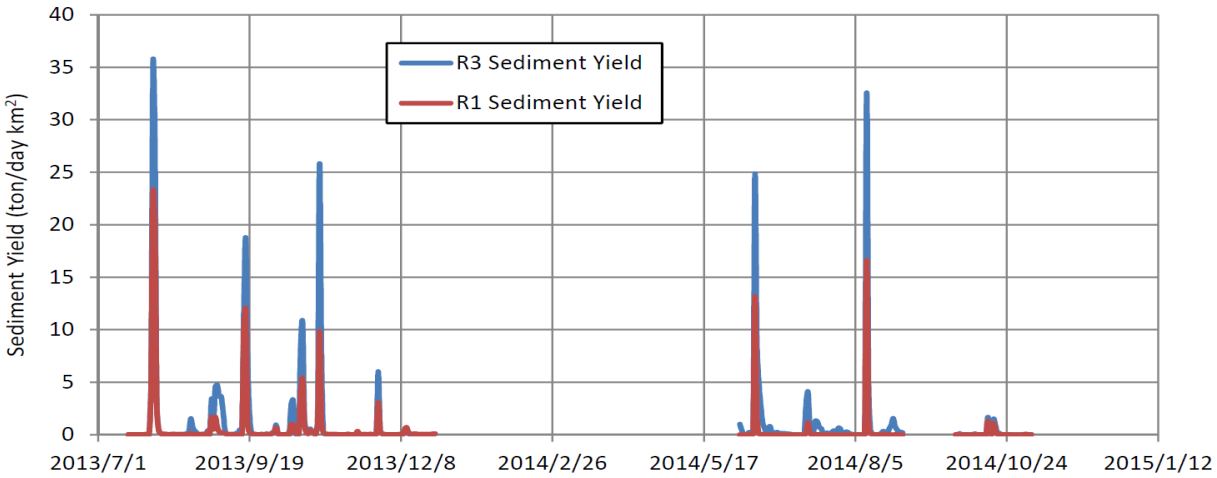


**Fig. 5.3** Sediment yield at site R1 and site R3

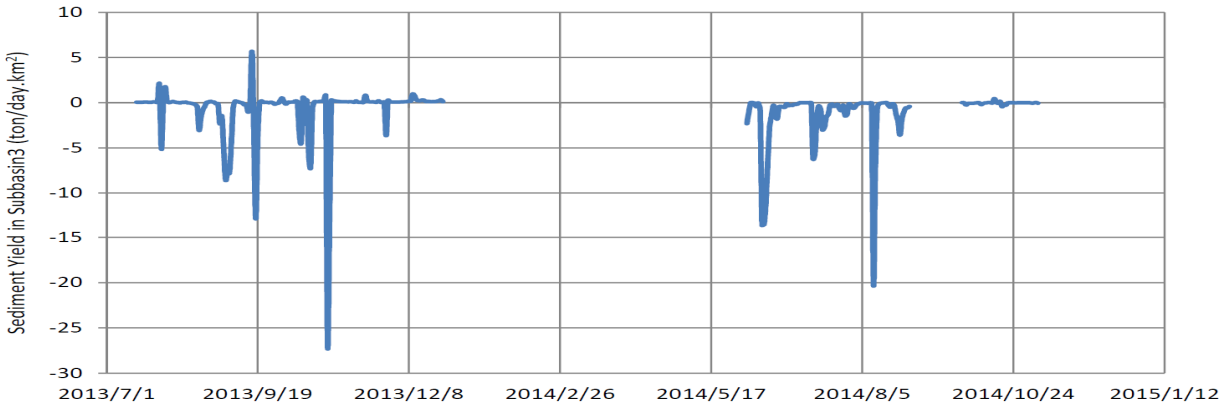


**Fig. 5.4** Sediment yield in subbasin 3

## 5.2 Rainfall Runoff events sediment yield at site R1 and R3

Runoff events sediment yield at site R1and site R3 in July 2013 – November 2014 are shown in **Figure 5.5**. Runoff events with extra sediment supply are found more times at site R3 than at site R1 in this period. At site R1 we observed 4 times runoff events with extra sediment supply whereas at site R3 12 times that is runoff events with extra sediment supply at site R3

three times more than that of R1 and the sediment yield in runoff event at site R1 is 1.4 times higher than R3, here the runoff events with extra sediment supply at site R1 are very few to get the proper regression line. Since the number of slope failure evens at site R3 is more than that of site R1 so here we can say slope failure frequently occur at upstream of site R3

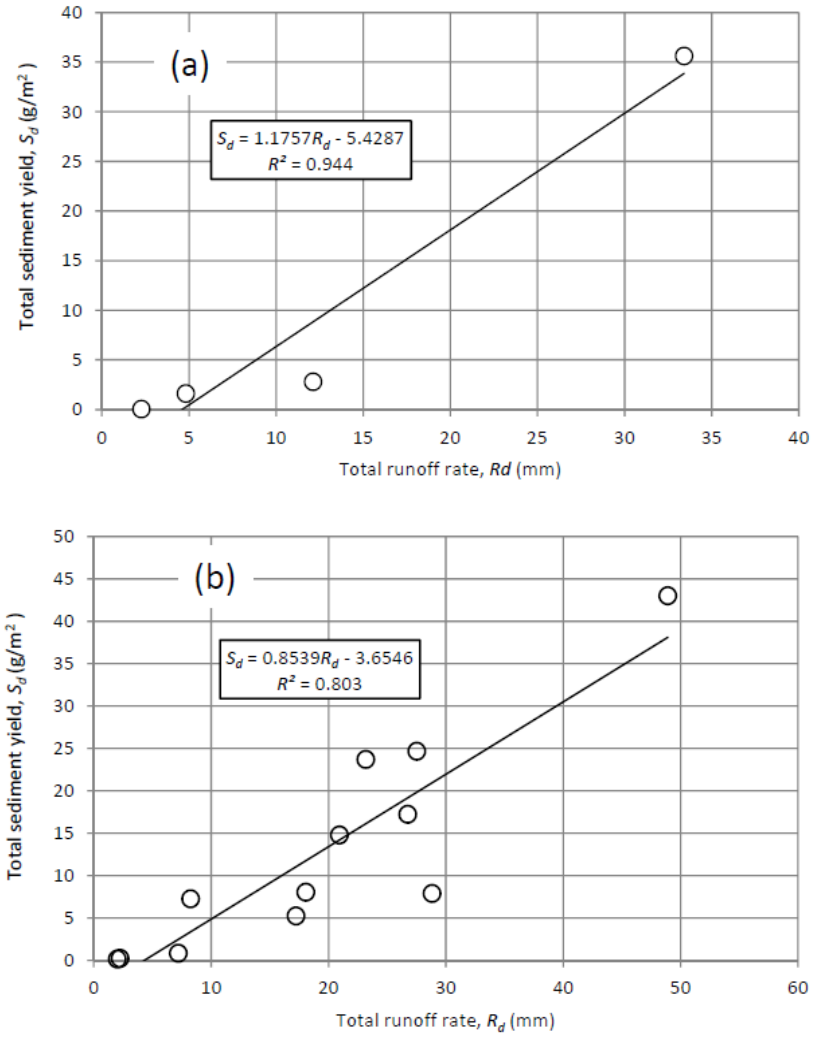


**Fig. 5.5** Relations between total runoff rate $R_d$ (mm) and total sediment yield $S_d$ (g m$^{-2}$) for rainfall runoff events with extra sediment supply (a) at site R1 (b) at site R3 in July 2013-2014.

**Figure 5.6** shows the total sediment yield at site R1 (**Fig. 5.6(a)**) and site R3 (**Fig. 5.6 (b)**) in the

runoff events without extra sediment supply. Numbers of runoff events at site R1and R3 are 12 and 6 respectively and the sediment yield at site R3 is 1.49 times higher than that of R1. It indicates that between site R3 and R1 no erosion but deposition is occurred.

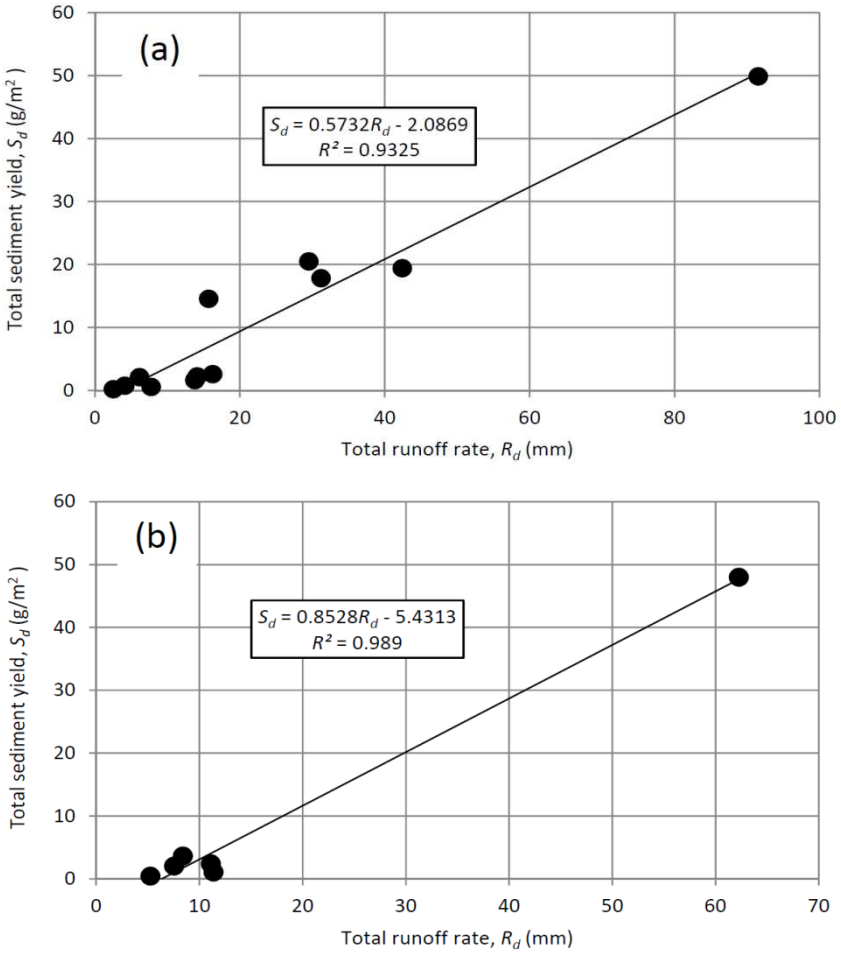


**Fig. 5.6** Relations between total runoff rate $R_d$ (mm) and total sediment yield $S_d$ (g m$^{-2}$) for rainfall runoff events without extra sediment supply (a) at site R1 (b) at site R3 in July 2013-2014.

### 5.3 Sediment load in different subbasin by SWAT model

I divided the forested Oikamanai River catchment into 3 subbasins (**Fig. 5.1**) based on elevation, soil type, land use and slope classes. SWAT model has simulated sediment load at every subbasin which is shown in **Figure 5.7**. We see that sediment load and sediment yield at

subbasin 2 (**Figure 5.7(a), (b)**) is always greater than subbasin 1 and subbasin 3 and most of the time sediment yield in subbasin 3 is negative (**Figure 5.7 (c)**); similar scenario was seen in monitoring observational data (**Figure 5.4**) which means that sediment deposition occurs between site R3 and site R1.

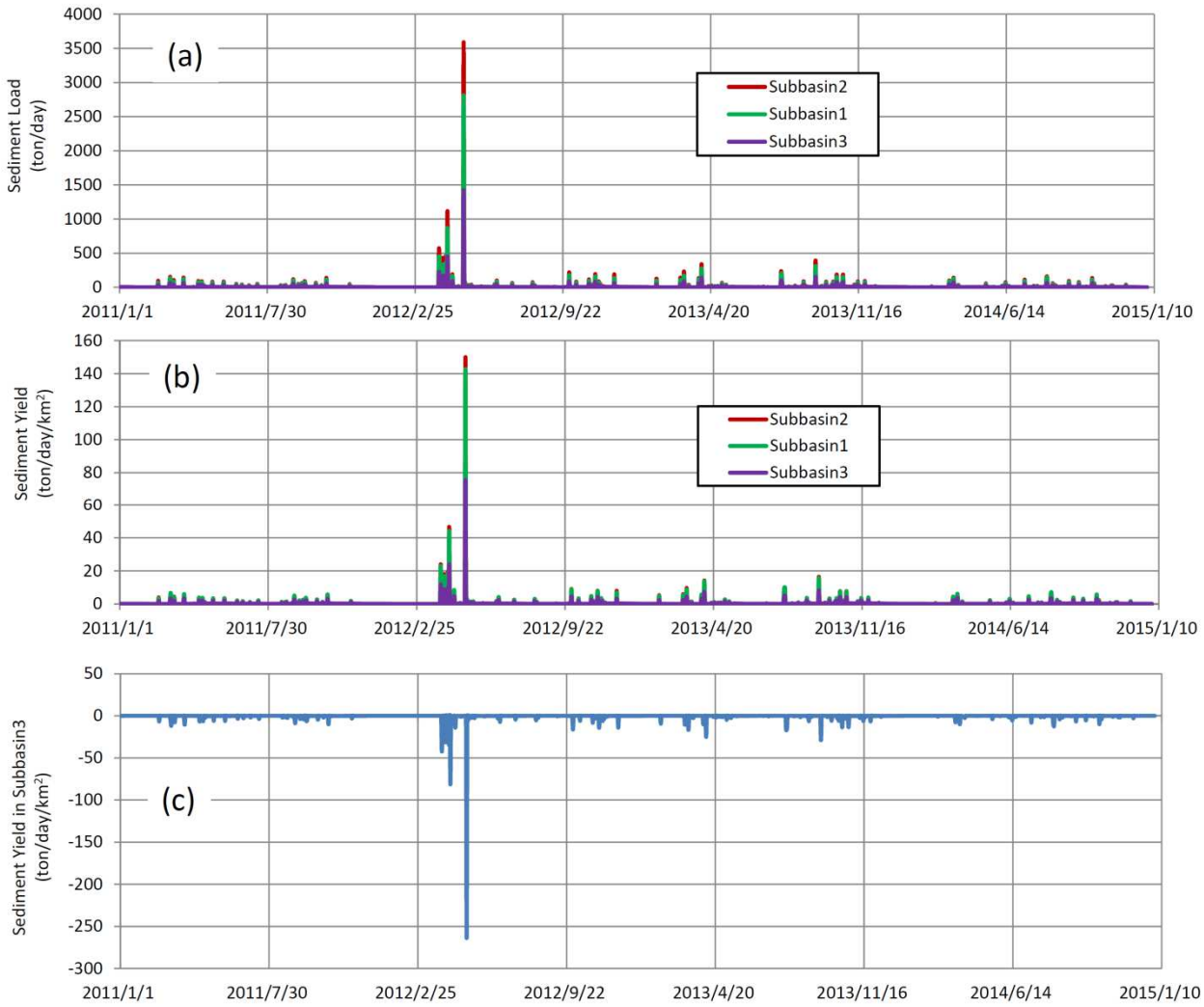


**Fig. 5.7** Sediment load and sediment yield (a) sediment load in three subbasin (b) sediment yield in three subbasin and (c)sediment yield in subbasin 3.

# CHAPTER SIX

## CONCLUSIONS

Hourly and daily time series of discharge, SSC and sediment load were obtained in the forested Oikamanai River catchment influenced by slope failure. The extra sediment supply to the river channel, probably from bank collapse or land slide, was found in fifteen runoff events by hourly discharge and SSC time series in 2011-2014. The total sediment yield in g $m^{-2}$ for the fifteen runoff events was about 2.8 times more than that for the events without extra sediment supply at site R1. The number of runoff events with extra sediment load supply at site R3 is three times more than at site R1 with sediment yield 1.46 times larger at site R1 than R3 whereas runoff events without extra sediment supply at site R1 is two times more than R3 though sediment yield at site R3 is 1.49 times greater than R1. Moreover sediment load at site R3 is always greater than that of at site R1 though discharge at site R1 is more that at site R3. In addition the most of the time sediment yield between sites R3 and R1 is negative. So the above phenomena indicate landslide or bank collapse frequently could occur at upstream of site R3 and sediment is deposited between sites R3 and site R1.

Daily discharge and sediment load time series were simulated by the lumped tank model and its coupling with power function. Simulated results of discharge are very reasonable with the Nash-Sutcliffe efficiency coefficient, *NSE* = 0.891 for calibration and 0.74–0.804 for validation years. Discharge simulation indicates that relatively large groundwater leakage occurs, especially in 2013, and in 2012 because of the large snowmelt amount and probably results from the high permeability of sedimentary bedrock with active faults. Sediment load simulation indicates that sediment erosion and transport by surface flow and river flow contribution are greater in year 2011 and 2012 are 91.3 % and 50.6 %. The sensitivity analysis for simulation pointed out that

investigations about behaviors of surface flow on the catchment slope are important to understand discharging and sediment-loading processes in the catchment.

From the observed and SWAT model simulation output we can apparently say that sub-basin 2 is the main sediment sources of this study area. Most of the sediment is deposited between sites R3 and R1 that is in subbasin 3. Most of the bank collapse and land slide events occur at the upstream of site R3 under rainfall from catchment slope and riparian region in this geologically active forested catchment which affects model calibration. A definitive interpretation of the quantitative results may not be appropriate because some processes are not well represented in the SWAT Model and lack of model parameterization at a local scale. While this study is able to give relative estimates of erosion measures, further model parameterization at a local scale should be done as more data and information become available.

# ACKNOWLEDGEMENTS

I would like to express my profound gratitude and praises to the Almighty Allah for all good graces and mercies he granted me in my life and career.

First and foremost, I would like to express my sincere gratitude and appreciation to my supervisor, Professor Dr. Kazuhisa A. Chikita for providing me the necessary platform and for giving me ample academic freedom to conduct my PhD thesis. And also for his consistent guidance, invaluable and constructive advice, patience and kindness. I will always be indebted to him in my academic career. I could not complete my doctoral thesis without a lot of his advices and supports.

My special thanks go to my jury members: Professor Dr. M. Nakatsugawa, Professor Dr. S. Minobe, Professor Dr. M. Furuya, and Professor Dr. M. Inatsu for their willingness to review and evaluate my thesis. Their valuable comments and suggestions helped me to improve the standard of this PhD thesis.

I would like to extend my thank Dr. Sakata Yoshitaka for his kind help and valuable advice to do my research work.

My great thanks go to my colleagues and friends at Laboratory of Physical Hydrology, especially to Wataru Iwasaka, Abdullah Al Mamun, Mimura Satoru, Miyanmoto Takuto, Ochiai Yasuhiro, Hiroyuki Uyehara, Makino Syou, Maeda Shingo, Yanaba Daisuke and Shibata Hiroiki who had a great impact to increase my theoretical and technical knowledge.

I would like to thank Hokkaido University for giving the financial support (Hokkaido University Special Grant Fellowship award) of my research work.

We are indebted to the Government of the Taiki-city and Fishermen’s Union at Hama-Taiki

Village for the kind permission of our field observations in the Oikamanai River. We express our gratitude to the farmers, Messrs. Mori and Takahashi, at the Seika Village for their frequent water sampling and instrument management. This study was supported partly by the Grant for Joint Research Program of the Institute of Low Temperature Science, Hokkaido University.

Last but definitely not least, I am extremely grateful to all the members of my family especially to my mother Jahanara Begum and my beloved wife Nousheen Parven for supporting me throughout this whole endeavor. I would not have gone so far without their unfailing support and encouragement.

# REFERENCES


Abbaspour K. C., 2007. User Manual for SWAT-CUP, SWAT Calibration and Uncertainty Analysis Programs, Swiss Federal Institute of Aquatic Science and Technology, Eawag, Duebendorf, Switzerland, 103 p.

Aksoy, H. & Kavvas, M. L., 2005 A review of hillslope and watershed scale erosion and sediment transport models. Catena 64, 247–271.

Araiba K., Nozaki T., Jeong B. & Fukumoto Y., 2008 Distribution of landslides and their geological characteristics in Japan. J. of the Jpn. Landslide Soc. 44, 37-44

Arnold J. G., Moriasi D. N., Gassman P. W., Abbaspour K. C., White M. J., Srinivasan R. and Jha M. K., 2012. SWAT: model use, calibration, and validation. Trans. ASABE, 55, 1491–1508.

Asselman, N. E. M., 1999. Suspended sediment dynamics in a large drainage basin: the River Rhine. Hydrological Processes 13, 1437-1450.

Babel M. S., Shrestha B. and Perret S., 2011. Hydrological impact of biofuel production: a case study of the Khlong Phlo Watershed in Thailand. Agric. Water Manage., 101, 8–26.

Baker, V. R., 1987. Regional landforms analysis. In "*Geomorphology from space: A global overview of regional landforms*" eds. by Short, N. M., Blair, Jr., R. W., Geocarto International, 2, 718pp.

Bagnold R. A., 1977. Bed load transport by natural rivers. Water Resour. Res., 13, 303–312.

Banks, D & Robins, N., 2002. An introduction to groundwater in crystalline bedrock. Geological Survey of Norway, ISBN 82 7386 100 1, 68pp.

Boithias L., Sauvage S., Taghavi L., Merlina G., Probst J. L. and Sa´ nchez-Pe´rez J.M., 2011. Occurrence of metolachlor and trifluralin losses in the Save River agricultural catchment during floods. J. Hazard. Mater., 196, 210–219.

Boithias L., Srinivasan R., Sauvage S., Macary F. and Sa´ nchez-Pe´rez J.M., 2013. Daily nitrate losses: implication on long-term river quality in an intensive agricultural catchment (south-western France). J. Environ. Qual., 43, 46–54.

Campbell, G. S. & Norman, J. M., 1998. *An Introduction to Environmental Biophysics*. Springer, 286pp.

Cerro I., Sa´ nchez-Pe´rez J. M., Ruiz-Romera E. and Antigu¨ edad I., 2013. Variability of particulate (SS, POC) and dissolved (DOC, NO3) matter during storm events in the Algeria agricultural watershed. Hydrol. Process., 28, 2855–2867.

Cerro I., Antigu¨ edad I., Srinivasan R., Sauvage S., Volk M. and Sa´ nchez-Pe´rez J.M., 2014. Simulating land management options to reduce nitrate pollution in an agricultural watershed dominated by an alluvial aquifer. J. Environ. Qual., 43, 67–74.

Chikita, K. A., Iwasaka, W., Mamun, A. A., Ohmori, K., Itoh, Y., 2012. The role of groundwater outflow in the water cycle of a coastal lagoon sporadically opening to the ocean. Journal of Hydrology, 464-465, 423-430.

Chikita, K. A., Uyehara, H., Mamun, A. A., Pascalis, F. D., Umgiesser, G., Iwasaka, W., Hossain, D. M. & Sakata, Y., 2015. Water and heat budgets in a coastal lagoon controlled by groundwater outflow to the ocean. Limnology, 16, 149–157.

Chow, V. T., Maidment, D. R., and Mays, L. W. 1988. Appl. Hydrol., McGraw-Hill, Singapore,.

Chu T. W., Shirmohammadi A., Montas H. and Sadeghi A., 2004. Evaluation of the SWAT model's sediment and nutrient components in the Piedmont physiographic region of Maryland. Trans. ASAE, 47, 1523–1538.

Easton Z. M., Fuka D. R., White E. D., Collick A. S., Biruk Ashagre B., McCartney M., Awulachew S. B., Ahmed A. A. and Steenhuis T. S., 2010. A multi basin SWAT model

analysis of runoff and sedimentation in the Blue Nile, Ethiopia, Hydrol. Earth Syst. Sci., 14, 1827–1841.

Ekstrom G., Stark C. P., 2013. Simple scaling of catastrophic landslide dynamics. Science, 339 6126, 1416-1419.

Francis X. A., McDonald G. N., 2010. Geologic characteristics and movement of the Meadow creek landslide, part of the Coal Hill landslide complex, Western Kane county, Utah. Utah geological association publication, 39, 38-60.

Gao P., 2008. Understanding watershed suspended sediment transport. Prog. Phys. Geog., 32, 243–263.

Haag I., Kern U. and Westrich B., 2001. Erosion investigation and sediment quality measurements for a comprehensive risk assessment of contaminated aquatic sediments. Sci. Total Environ., 266, 249–257.

Heathwaite A. L., Dils R. M., Liu S., Carvalho L., Brazier R. E., Pope L., Hughes M., Philips G. and May L., 2005. A tiered risk-based approach for predicting diffuse and point source phosphorus losses in agricultural areas. Sci. Total Environ., 344, 225–239.

Hossain, M. M., Chikita, K. A., Sakata, Y., Miyamoto, T. & Ochiai, Y., 2015. Groundwater Leakage and River Runoff in a Catchment Influenced by Tectonic Movement. Open Journal of Modern Hydrology, 5, 32-44.

Jayakrishnan R., Srinivasan R., Santhi C. and Arnold J.G., 2005. Advances in the application of the SWAT model for water resources management. Hydrol. Process., 19, 749–762.

Kerr J. G., Burford M. A., Olley J. M., Bunn S. E. and Udy J., 2011. Examining the link between terrestrial and aquatic phosphorus speciation in a subtropical catchment: the role of selective erosion and transport of fine sediments during storm events. Water Res., 45, 3331–3340.

Kido, D., Chikita, K. A., and Hirayama, K., 2007. Subglacial drainage system changes of the Gulkana Glacier, Alaska: discharge and sediment load observations and modeling. Hydrological Processes, 21: 399–410.

Kim J. G., Park Y. S., Yoo D., Kim N., Engel B. A., Kim S., Kim K. S. and Lim K.J., 2009. Development of a SWAT patch for better estimation of sediment yield in steep sloping watersheds. J. Am. Water Resour. Assoc., 45, 963–972.

Kondo, J., 1998. Meteorology in Aquatic Environments. 2nd ed., Asakura Publication, Inc., Tokyo, 350pp.

Lal R., 1998. Soil erosion impact on agronomic productivity and environment quality. Crit. Rev. Plant Sci., 17, 319–464.

McCullough, M. C., Eisenhauer, D. E., Dosskey, M., 2008. Modeling runoff and sediment yield from a terraced watershed using WEPP. USDA Forest Service / UNL Faculty Publications, Paper No. MC08-118, 12pp, University of Nebraska Lincoln.

Merritt, W. S., Letcher , R. A. & Jakeman, A. J., 2003. A review of erosion and sediment transport models. Environmental Modelling & Software 18, 761–799.

Michalski, A. & Britton, R., 1997. The role of bedding fractures in the hydrogeology of sedimentary bedrock-evidence from the Newark Basin, New Jersey. *Ground Water*, 35, 318-327.

Morgan, R. P. C., 1995. Soil Erosion and Conservation. 2nd edition. London: Longman.

Mukundan R., Radcliffe D. E. and Risse L.M., 2010. Spatial resolution of soil data and channel erosion effects on SWAT model predictions of flow and sediment. J. Soil Water Conserv., 65, 92–104.

Morgan R. P. C., Quinton J.N., Smith R. E., Govers G., Poesen J. W. A., Auerswald K., Chisci G., Torri D. and Styczen M.E., 1998. The European soil erosion model (EUROSEM): a

dynamic approach for predicting sediment transport from fields and small catchments. Earth Surf. Proc. Land., 23, 527–544.

Nash, J. E. & Sutcliffe, J. V., 1970. River flow forecasting through conceptual models part I - A discussion of principles. Journal of Hydrology, 10, 282–290.

Nearing M. A., Foster G. R., Lane L. J. and Finkner S. C., 1989. A process-based soil erosion model for USD-Water Erosion Prediction Project Technology. Trans. ASAE, 32, 1587–1593.

Oeurng C., Sauvage S. and Sa´ nchez-Pe´rez J. M., 2011. Assessment of hydrology, sediment and particulate organic carbon yield in a large agricultural catchment using the SWAT model. J. Hydrol., 401, 145–153.

Phomcha P., Wirojanagud P., Vangpaisal T. and Thaveevouthti T., 2011. Predicting sediment discharge in an agricultural watershed: a case study of the Lam Sonthi watershed, Thailand. Science Asia, 37, 43–50.

Qiu, L., Zheng, F., Yin, R., 2012. SWAT-based runoff and sediment simulation in a small watershed, the loessial hilly-gullied region of China: capabilities and challenges. International Journal of Sediment Research, 27, 226-234.

Saghafian B., Sima S., Sadeghi C. and Jeirani F., 2012. Application of unit response approach for spatial prioritization of runoff and sediment sources. Agric. Water Manage., 109, 36–45.

Santhi C., Arnold J.G., Williams J.R., Dugas W.A., Srinivasan R. and Hauck L.M., 2001. Validation of the SWAT model on a large river basin with point and nonpoint sources. J. Am. Water Resour. Assoc., 37, 1169–1188.

Seaton, W. & Burbey, T. J., 2005. Influence of ancient thrust faults on the hydrogeology of the blue ridge province. Groundwater, 43, 301-313.

Stamos, C. L., Cox, B. F., Izbicki & Mendez, G.O., 2003. Geologic Setting, Geohydrology and

Ground- Water Quality near the Helendale Fault in the Mojave River Basin, San Bernardino County, California. *USGS Water-Resources Investigations Report* 03-4069, 44pp.

Sugawara, M., 1972. *A Method for Runoff Analysis*. Tokyo Kyoritsu Shuppan Press (in Japanese).

Talebizadeh, M., Morid, S., Ayyoubzadeh, S. A. & Ghasemzadeh, M., 2010. Uncertainty analysis in sediment load modeling using ANN and SWAT model. Water Resources Managements 24, 1747–1761.

Tanaka, S., Takeda, H., Iwata, T., Tsuchiya, T. & Terao, M., 2006. Architectural Environmental Engineering. 3rd edition, Inoue Publ. Inc., Japan, 324pp.

Thomas R. B., 1988. Monitoring baseline suspended sediment in forested basin: the effect of sampling on suspended sediment rating curves. Hydrol. Sci. J., 33, 499–514.

Tsai, T. L., Yang. J. C., 2012. Modeling of rainfall-triggered shallow landslides. Environmental geology, 5, 525-534.

Van Rompaey, A. J. J., Verstraeten G., Van Oost K., Govers G. and Poesen J., 2001. Modelling mean annual sediment yield using a distributed approach. Earth Surf. Proc. Land., 2, 1221–1236.

Wada, T., Chikita, K. A., Kim, Y. & Kudo, I., 2011. Glacial Effects on Discharge and Sediment Load in the Subarctic Tanana River Basin, Alaska. Arctic, Antarctic, and Alpine Research, 43(4):632-648.

Walling, D. E., 1974. Suspended sediment and solute yields from a small catchment prior to urbanization. In Gregory, K. J., and Walling, D. E. (eds.), Fluvial Processes in Instrumented Watersheds. London, U. K.: Institute of British Geographers, Special Publication, 6: 169–192.

Walling, D. E., Webb, B. W., 1982. Sediment availability and the prediction of storm-period sediment yields. IAHS Publ. no. 137, 327-337.

Williams J.R., 1975. Sediment routing for agricultural watersheds. J. Am. Water Resour. Assoc., 11, 965–974.

Zˆezere, J. L., R. M. Trigo and I. F. Trigo (2015): Shallow and deep landslides induced by rainfall in the Lisbon Region (Portugal): Assessment of relationships with the North Atlantic Oscillation", Natural Hazards and Earth System Sciences, 5, 331–344.